Colloquium: Optimal control of high-harmonic generation

Carsten Winterfeldt, Christian Spielmann,* and Gustav Gerber

Universität Würzburg, Physikalisches Institut, 97074 Wuerzburg, Germany

(Published 2 January 2008)

High-harmonic generation provides an attractive light source of coherent radiation in the extreme-ultraviolet (XUV) and soft-x-ray regions of the spectrum and allows for the production of single attosecond pulses or pulse trains. This Colloquium covers the control of high-harmonic spectra by temporal and spatial pulse shaping of the driving laser pulses and its implications on time-resolved XUV spectroscopy and attosecond pulse shaping. It summarizes important steps for extending existing pulse shaping techniques and control schemes from the near-infrared or visible part to shorter wavelengths. Using adaptive pulse shaping of the driving laser pulses, several groups have demonstrated control of the high-harmonic spectrum, including the author's work on the complete control over the XUV spectrum of high-order harmonics, generated in a gas-filled hollow fiber. It is possible to achieve both the enhancement and the suppression of single or several selected harmonic orders. These arbitrarily shaped soft-x-ray spectra will allow for important modifications of the resulting harmonic pulses in the temporal domain. This constitutes first steps towards direct attosecond pulse shaping in the soft-x-ray domain. Moreover, high-harmonic generation in a hollow-core fiber can be enhanced by coupling into a single fiber mode using a feedback-controlled adaptive two-dimensional spatial light modulator.

DOI: 10.1103/RevModPhys.80.117 PACS number(s): 37.10.Jk, 42.65.Ky, 42.79.Nv, 42.65.Re

CONTENTS

I. Introduction 117
II. High-Harmonic Generation 119
A. Single-atom response (three-step model) 119
B. Harmonic spectrum 121
C. Propagation and phase matching 122
D. Attosecond pulse generation 124
E. Coherence 124
F. Challenges and goals 125
III. Adaptive Control 126
IV. Control of High-Harmonic Generation Through Temporal Laser Pulse Shaping 127
A. Open-loop control 128
B. Tailoring high-harmonic spectra by adaptive temporal pulse shaping (closed-loop control) 129
1. Adaptive optimizations in gas jets 129
2. Enhanced control in hollow fibers 130
V. Control of High-Harmonic Generation Through Spatial Engineering 132
A. Free-focusing geometry 132
B. Fiber-mode excitation 133
C. Optimizations in a hollow-core fiber 133
D. Optimizing the geometry: Quasi-phase-matched generation 134
E. Optimizing the medium 135
VI. High-Harmonic Time Structure 135
VII. Conclusion 137
Acknowledgments 137
References 137

*spielmann@physik.uni-wuerzburg.de

I. INTRODUCTION

Femtosecond laser technology has enabled us to follow atomic motion in real time (Rose *et al.*, 1988; Baumert *et al.*, 1991) which has been recently reviewed by Zewail (2000) and to control molecular processes (Judson and Rabitz, 1992; Bardeen *et al.*, 1997; Assion *et al.*, 1998; Weinacht *et al.*, 1999; Brixner *et al.*, 2001; Levis *et al.*, 2001; Herek *et al.*, 2002) with tailored femtosecond laser pulses (Weiner *et al.*, 1990; Judson and Rabitz, 1992; Baumert *et al.*, 1997; Yelin *et al.*, 1997; Weiner, 2000). The vibrational periods of atoms in molecules, which reflect the intramolecular *atomic* dynamics, lie in the range of tens to hundreds of femtoseconds. Laser pulses with durations of this order of magnitude can therefore efficiently measure and control molecular dynamics. However, the natural time scale of *electrons* falls into the subfemtosecond or attosecond regime. Important electronic processes include charge transfer after excitation or atomic inner-shell transitions. In order to explore electronic motion in real time as well as to control electronic dynamics, it is therefore desirable to develop new light sources with energies in the extreme-ultraviolet (XUV) region and pulse durations of the order of attoseconds to be able to directly access core-level electrons easily with one-photon transitions and with laboratory-scale experimental setups. State-of-the-art femtosecond laser systems are usually based on Ti:sapphire technology, implying an operational laser wavelength of 800 nm in the near infrared, limiting the shortest attainable laser pulse duration to about 2.6 fs (one complete oscillation cycle), almost reached by recent experiments (Yamane *et al.*, 2003). For shorter pulse durations in the subfemtosecond regime, shorter wavelengths have to be used. The energetic scale of core electronic

transitions also necessitate photons in the XUV.

Several techniques can be used to reach this wavelength range. Laser-produced plasmas (LPP) are created by the interaction of a high-intensity laser pulse with high-density materials, leading to the emission of both bremsstrahlung and characteristic line radiation (Giulietti and Gizzi, 1998; Schwoerer, 2004). This radiation has durations on the subpicosecond to femtosecond scale and is intrinsically synchronized to the external laser source that generated the plasma. As a drawback, the radiation is incoherent and is emitted into a large solid angle. Spatially and coherent emission at selected wavelengths in the soft x-ray range can be obtained with a LPP driven x-ray laser. These sources have been recently extensively reviewed by Daido (2002) and Tallents (2003).

This problem is resolved in undulator-based free-electron lasers (FEL) (Andruszkow *et al.*, 2000), where the buildup of the x-ray pulses is coherent, leading to much higher fluxes in the forward direction. Photons at 12.7 eV (98 nm) from the Tesla Test Facility (TTF-FEL) at DESY have been used to examine the multiple ionization of atom clusters (Wabnitz *et al.*, 2002). Recently, the operation of the free-electron laser at 32 nm (38.8 eV) has been demonstrated (Ayvazyan *et al.*, 2006).

To perform the far-reaching step towards attosecond laser pulse production and application [labeled "the transition from femtochemistry to attophysics" by Silberberg (2001)] a different approach is needed. Based on highly nonlinear effects accessible with high-power femtosecond laser systems, this can be realized by the generation of high-order harmonics of the driving laser (Li *et al.*, 1989; L'Huillier and Balcou, 1993; Macklin *et al.*, 1993), leading to coherent emission in the soft-x-ray range.

Since the invention of the laser in 1960 by Theodore Maiman (1960), attainable laser pulse durations have decreased from several hundreds of microseconds in the ruby laser down to less than 10 fs at very high peak powers and intensities in modern femtosecond Ti:sapphire laser systems (Bloembergen, 1999). This allows the use of nonlinear optical techniques to convert existing laser light frequencies to different frequencies where standard light sources with the desired properties (e.g., wavelength, pulse duration, intensity, polarization) do not exist. The first application of the red ruby laser at 694.3 nm successfully produced blue 347.2 nm radiation through the process of second-harmonic generation (Franken *et al.*, 1961). When a strong electric field (as from this pulsed laser) is applied to a medium, polarization in the medium exhibits contributions not only at the original frequency (linear response) but terms of second, third, or higher order in the driving electric field appear, resulting in the generation of light at the corresponding integer multiples of the frequency of the incident light.

Further advances in femtosecond laser technology do not only allow for these low-order nonlinear processes such as second-harmonic or third-harmonic generation, but they make it possible to exploit the highly nonlinear response of atoms and other media in high-intensity laser fields to generate very-high-order harmonics of the fundamental laser frequency (high-harmonic generation). This new electromagnetic radiation at much shorter wavelengths than the original optical pulse (at visible and near-infrared wavelengths) was found accidentally over a decade ago when researchers used intense femtosecond laser pulses to ionize rare gases (McPherson *et al.*, 1987; Li *et al.*, 1989; L'Huillier and Balcou, 1993; Macklin *et al.*, 1993).

High-harmonic generation provides a powerful source of ultrashort coherent radiation in the XUV and soft-x-ray range and has the inherent advantage to be realizable on a laboratory scale (so-called table-top systems) as opposed to large free-electron-laser facilities. Recent experiments have proven the existence of high-harmonic-based attosecond laser pulses by characterizing the temporal structure of the high-order harmonics (Antoine *et al.*, 1996; Christov *et al.*, 1997; Drescher *et al.*, 2001; Hentschel *et al.*, 2001; Paul *et al.*, 2001; Mairesse *et al.*, 2003; Agostini and DiMauro, 2004). Several groups (Nugent-Glandorf *et al.*, 2001; Drescher *et al.*, 2002; Kienberger *et al.*, 2002, 2004; Scrinzi *et al.*, 2006) have exploited the unique temporal properties of this new radiation to examine electronic dynamics, for example, the Auger decay of innershell electrons. The attosecond time domain had not been directly accessible before due to the lack of such extremely short light pulses. It is now up to the researchers to make further use of this novel light source which has the potential for a large number of seminal discoveries. Since the exploration and observation of processes in turn are accompanied with the desire to control them, it is the scope of this work to demonstrate ways to manipulate the properties of these soft-x-ray pulses.

In general, for multicycle linearly polarized femtosecond laser pulses in a centrosymmetric medium conventionally used, high harmonics are produced at each half-cycle of the electric field of a laser pulse and are therefore emitted as light bursts with a periodicity of half a laser period. Combined analysis of the reciprocity properties of the Fourier transform and of the observation of the sign flip between consecutive bursts shows that the full harmonic spectrum usually consists of the odd harmonics of the fundamental laser frequency (Salières *et al.*, 1998; Mauritsson *et al.*, 2006). For spectroscopic applications, it is desirable to use a single harmonic to facilitate the interpretation of the acquired data. The selection of single harmonics with a grating is accompanied with a loss of time resolution due to dispersion and with a substantial intensity reduction due to low reflectivities. As a superior alternative, existing laser pulse shaping techniques can be used to control the high-harmonic spectrum and engineer harmonics as needed. A number of experiments have been performed with the goal of influencing the harmonic spectra, which is summarized here to cover the field of the control of high-harmonic radiation to a certain level of completeness.

We have demonstrated the comprehensive control of high harmonics (Pfeifer, Kemmer, *et al.*, 2005; Pfeifer,

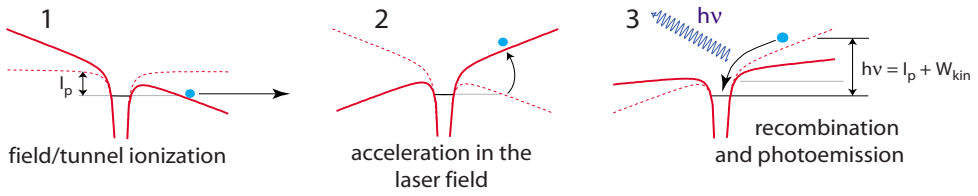

FIG. 1. (Color online) Illustration of the three-step model for high-harmonic generation: (1) tunnel ionization of the electron, (2) acceleration in the laser electric field, and (3) recombination and emission of a high-energy photon. The energy of the emitted photon depends on the ionization potential of the atom and on the kinetic energy of the electron upon its return to its parent ion.

Walter, *et al.*, 2005), including both the enhancement and suppression of single or multiple selected harmonic orders by temporal pulse shaping. These tunable quasimonochromatic high-harmonic spectra allow for time-resolved spectroscopy in the soft-x-ray region and are therefore of great importance to a broad field of scientific disciplines. Arbitrarily shaped soft-x-ray spectra will also allow for major modifications of the resulting harmonic pulses in the temporal domain which paves the way towards direct attosecond pulse shaping and optimal control in the soft-x-ray domain.

In addition to the temporal shaping of the electric field of the driving laser pulse, the influence of spatial properties such as propagation effects is examined using a feedback-controlled adaptive two-dimensional spatial light modulator. High-harmonic generation in a hollow-core fiber can be enhanced by coupling into a single fiber mode. These results resolve the long-standing issue on the limited controllability of high-harmonic generation in free-focusing geometries such as gas jets (Yoshitomi *et al.*, 2003; Reitze *et al.*, 2004; Villoresi *et al.*, 2004) as compared to geometries where the laser is guided (Bartels *et al.*, 2000, 2001). Complete control over the shape of the soft-x-ray spectrum has a major impact on ultrafast energy-resolved spectroscopy and on the temporal structure of high harmonics. The results presented in this Colloquium therefore have direct implications for fields such as time-resolved XUV spectroscopy, nonlinear optics, biology, and chemistry in the soft-x-ray-range.

This Colloquium is organized as follows: Section II introduces high-harmonic generation in more detail. Emphasis is put on the different aspects of high harmonics, such as their unique generation mechanism, the harmonic spectrum and attosecond pulse generation, coherence, and high-harmonic phase matching. The following section (Sec. III) discusses the scheme of adaptive control. Sections IV and V summarize the experimental progress on the control of high-harmonic radiation mainly through temporal and spatial laser pulse shaping. Section VI reviews the temporal properties of high-harmonic bursts before the Conclusion completes the presentation of the achievements and progress made in the field of the control of high-harmonic radiation.

II. HIGH-HARMONIC GENERATION

As opposed to low-order nonlinear frequency conversion processes such as second-harmonic generation where moderate laser intensities are sufficient, high-order harmonics result from the highly nonlinear interaction of high-intensity laser pulses with typically a gaseous medium. Laser radiation is converted into large integer multiples of the original laser frequency [~300 (Spielmann *et al.*, 1997)], which reaches down to the XUV (extreme ultraviolet) and soft-x-ray range. In the following we describe high-harmonic generation in more detail.

A. Single-atom response (three-step model)

The basic generation mechanism for high-order harmonics can be explained using the semiclassical so-called simple-man model or three-step model by Corkum (1993) and Kulander *et al.* (1993) as summarized in Fig. 1. In the strong field of ultrashort high-intensity laser pulses, bound electrons from atoms or molecules are field ionized close to the maximum of the laser field [tunnel ionization (Keldysh, 1965; Ammosov *et al.*, 1986)] and set free with zero initial velocity. They are then accelerated away from their parent ions by the same electric field and move on classical electron trajectories in a laser field.

The average quiver energy of the electron in the laser field is called the ponderomotive energy U_p and is directly proportional to the intensity I of the driving laser and the square of the fundamental wavelength λ:

$$U_p = \frac{e^2 E_L^2}{4 m_e \omega_L^2} \propto I\lambda^2, \tag{1}$$

where e and m_e are the charge and the mass of the electron, and E_L is the electric field strength of the laser with the angular frequency ω_L (or wavelength λ).

In the three-step model, as soon as the electric field reverses, electrons are first decelerated and then accelerated back towards their parent ions, depending on the instant of birth into the continuum by ionization. Several processes can be realized when the electron returns to the core.

High-harmonic generation (HHG). The electron can recombine with its parent ion with a certain probability, leading to the emission of a broadband extreme-ultraviolet (XUV) photon. One photon per electron is emitted carrying the sum of the electron's kinetic energy plus the ionization potential I_p.

(High order) above-threshold ionization [(H)ATI].

Above-threshold ionization (ATI) originates from the elastic scattering of the electron with the atom. The electron gains energy in excess of its initial energy in integer multiples of the fundamental laser frequency (Agostini *et al.*, 1979; Freeman *et al.*, 1987; Paulus, Nicklich, *et al.*, 1994). A typical photoelectron spectrum shows a characteristic plateau of electron peaks, separated by one fundamental photon energy and rolling off at a cutoff of $10U_p$ (Paulus, Becker, *et al.*, 1994; Paulus, Nicklich, *et al.*, 1994; Milošević *et al.*, 2006). The position of the ATI peaks can be shifted by the ponderomotive potential or even be suppressed, depending on the pulse duration of the driving laser (Freeman *et al.*, 1987).

Nonsequential double ionization (NSDI). When an inelastic collision of the electron with its parent ion occurs, another electron can be ionized so that in the end the atom is doubly ionized [nonsequential double ionization (NSDI) (Fittinghoff *et al.*, 1992; Walker *et al.*, 1994)]. Inelastic colllsion processes are the dominant, but not the only mechanism for NSDI, other processes, e.g., shake-up, are known to play a role (Dorner *et al.*, 2004).

Here we are only interested in high-harmonic generation and the control of their spectral and temporal properties. The energy of the photon that is emitted upon recollision of the accelerated electron with the ion core is determined by the sum of the ionization potential I_p and the momentary kinetic energy W_{kin} of the electron:

$$\hbar\omega = I_p + W_{\mathrm{kin}}(\varphi). \tag{2}$$

The kinetic energy depends on the phase φ of the electric field at the moment of ionization. The maximum photon energy (cutoff energy) that can be achieved in this process can be calculated using classical (Corkum, 1993) or quantum mechanics (Lewenstein *et al.*, 1994) and is given by

$$E_{\mathrm{cutoff}} = \hbar\omega_{\mathrm{max}} = I_p + 3.17U_p, \tag{3}$$

where ω is the (angular) frequency of this photon and $\hbar$ is Planck's constant. The right-hand side of Eq. (3) is composed of the ionization potential I_p of the atom (the binding energy of the electron) and the maximum kinetic energy of the electron upon its return to the core: $3.17U_p$. This happens for a phase of $\varphi \approx 17°$ close to the maximum of the electric field where also the ionization rate is highest.

To visualize the laser intensities needed for a sizable ponderomotive potential U_p, Eq. (1) can be reformulated:

$$U_p(\mathrm{eV}) = 0.93 \times 10^{-13} I(\mathrm{W\ cm^{-2}})\lambda^2(\mu\mathrm{m}^2). \tag{4}$$

The corresponding laser intensities of 10^{16} W cm^{-2} are equivalent to an electric field amplitude of $E_L = 5 \times 10^9$ V cm^{-1}, which is a typical value of the inneratomic electric field.

Lower harmonic orders (long wavelengths) can usually be described using perturbation theory, predicting a decrease of harmonic intensities towards higher orders following an I^q power law. The exponential of this power law is given by the number of the corresponding harmonic order q. Perturbation theory breaks since the electric field of the laser approaches the inneratomic electric field. The effective exponential p in the modified power law I^p is smaller than q (Lompré *et al.*, 1990). Intermediate harmonic orders show a plateau in intensity (L'Huillier *et al.*, 1991) which ends at the cutoff energy for the highest harmonic orders (Fig. 1, upper panel).

According to Eq. (1), the cutoff can be extended to higher energies by using a longer-wavelength driving field (Shan and Chang, 2001; Tate *et al.*, 2007). On the other hand, the efficiency of high-harmonic generation is increased for shorter-wavelength pulses due to the reduced wave packet spreading of the electron during its excursion time (Tempea and Brabec, 2000). Also, since the oscillation amplitude of the electron in the laser field scales as λ^2, the electron spends more time in the vicinity of the atom for the shorter-wavelength driver and, therefore, has a larger probability of emitting a harmonic photon per unit time (Ditmire *et al.*, 1995).

An extension of the position of the cutoff is also possible by using a higher intensity driving laser pulse, provided that plasma effects such as dephasing and defocusing are properly controlled and not all atoms will be ionized in the leading edge of the pulse. Using few cycle laser pulses will substantially reduce the ionization probability prior to the maximum field strength in the center of the pulse, minimizing ground state depletion and plasma effects (Brabec and Krausz, 2000). Finally an increased intensity poses some limits on high-harmonic generation even in the single-atom limit. In high-intensity laser fields electrons may gain velocities of the order of the velocity of light. In this regime magnetic-field forces become comparable to electric-field forces. The electron follows a figure eight trajectory due to the contribution of the $\boldsymbol{v} \times \boldsymbol{B}$ terms induced by the strong magnetic-field components which leads to a significant motion of the electron in the propagation direction of the laser field. As a consequence, there is less interaction with the nucleus and very few harmonics can be found in the radiation spectrum (Keitel and Knight, 1995). Also, relativistic mass effects have to be taken into account, preventing the acceleration of the electron to even higher energies necessary for the extension of the cutoff.

Figure 2 shows a plot of different classes of electron trajectories during propagation in the electric field of the driving laser. Electrons start from the nucleus located at (0, 0). Depending on the phase Φ of the electric field at the instant of ionization, they can return to the core at position 0. The intersection with the velocity axis determines their final kinetic energies at the moment of recombination. The electron along the cutoff trajectory *b* was ionized at a phase of $\Phi = 17°$ and has the highest kinetic energy of $3.17U_p$ upon its return to the core. Electrons are most likely produced at the peak of the electric field ($\Phi = 0°$) but they return to the core with zero kinetic energy (*d*). Most electrons, however, are produced at unfavorable phases of the electric field and never return to the core (*e*). In the plateau region of

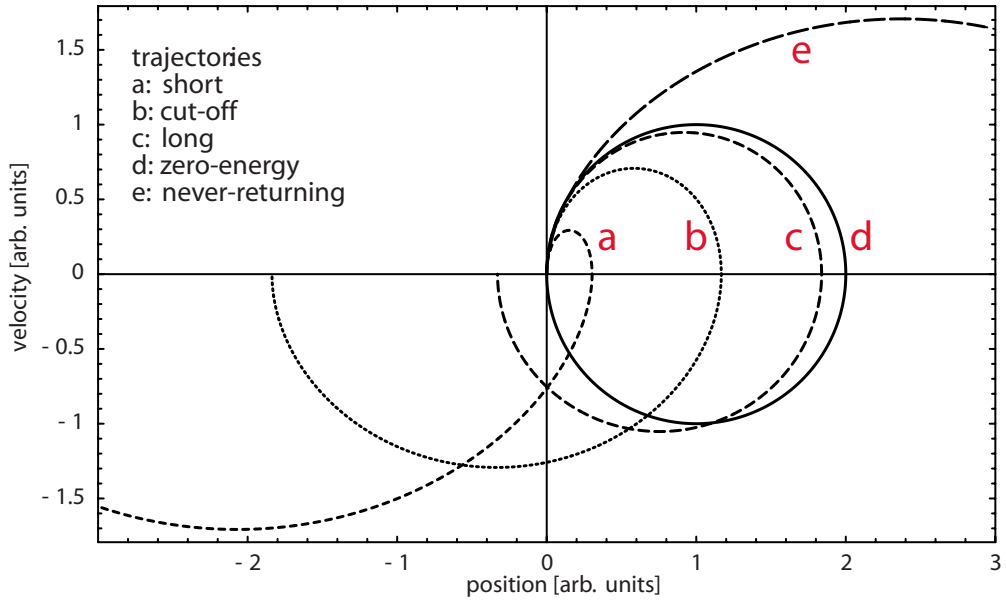

FIG. 2. (Color online) Different classes of electron trajectories during the propagation phase of high-harmonic generation, plotted in the position-velocity plane: The trajectories start at the atom located at (0, 0). Depending on the phase Φ of the electric field at the instant of ionization, they can return to the core at position 0 with different kinetic energies, visualized by the intersection with the velocity axis. The traces $a(\Phi=45°)$ and $c(\Phi=3°)$ correspond to the short and long trajectory, respectively, leading to the same final energy. Class $b(\Phi=17°)$ is a cutoff trajectory with the highest kinetic energy ($3.17U_p$), $d(\Phi=0°)$ starts at the peak of the electric field where most electrons are produced but returns to the core with zero kinetic energy. Trajectory $e(\Phi=-45°)$ never returns to its parent atom.

high-harmonic spectra, there are typically two electron trajectories that give dominant contributions to high-harmonic emission, which interfere with each other (Lewenstein *et al.*, 1995). The first short trajectory corresponds to a short return time (a), the second long trajectory (c) has a return time close to one period, which causes a strong intensity dependence of the phase. This can result in strong spectral broadening, leading to an overlap of neighboring peaks (Salières *et al.*, 1998).

The phase of the harmonic emission can be determined using a quantum-mechanical formulation, the so-called Lewenstein model (Lewenstein *et al.*, 1994, 1995). This theory rephrases the classical models by Corkum (1993) and Kulander *et al.* (1993) in a fully quantum theory. It is valid in the single-active-electron approximation (SAE) in a low-frequency, high-intensity limit ($U_p \geqslant I_p$), and for high harmonics with energies greater than the ionization potential.

Referring to Feynman's path integral formalism, Salières *et al.* (2001) expressed the probability amplitude for high-harmonic generation as a coherent superposition of contributions of all possible spatiotemporal paths that connect the initial and the final state of the system, the so-called quantum orbits. The weight of each path is a complex number whose phase is equal to the classical action S along this path. In general, only the first two quantum orbits with travel times of less than one or two periods of the laser field contribute noticably. For harmonics in the cutoff region, there is only one relevant trajectory whereas for plateau harmonics two trajectories are needed for an accurate description. The implications of the spatiotemporal separation of high-harmonic radiation into two quantum path components will be discussed in Sec. II.E on the coherence properties of high harmonics.

B. Harmonic spectrum

Since the generation of high-harmonic radiation is repeated every half-cycle of the electric field of the laser pulse, their spectrum consists of the odd harmonics of the fundamental laser frequency [Fig. 3 (schematical view)]. Each half-cycle of the driving laser pulse gives

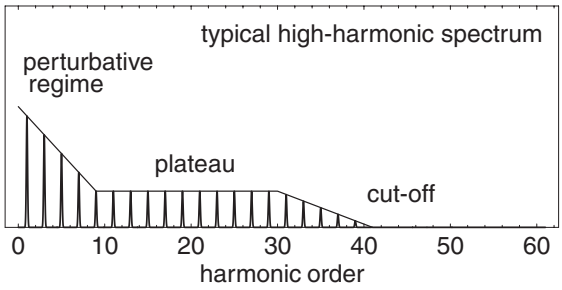

FIG. 3. Typical high-harmonic spectrum. The temporal periodicity of high-harmonic emission with half the laser oscillation period leads to a harmonic spacing of twice the fundamental frequency. The spectrum can be divided into three parts (which have been exaggerated in this schematic diagram for clarity): the perturbative regime at low orders, the plateau for intermediate orders, and the cutoff at the highest orders.

rise to a short (subfemtosecond) burst of XUV radiation. Therefore a driving pulse consisting of multiple cycles produces a train of subfemtosecond XUV bursts, separated in time by half the oscillation period of the driving laser [attosecond pulse train (APT) (Antoine *et al.*, 1996; Paul *et al.*, 2001; Tzallas *et al.*, 2003)]. This periodicity of $T/2$ (where T is the laser period) is responsible for the observation of the harmonic spacing of 2ω. This behavior can simply be understood from the reciprocity of the Fourier transform, through which the electric field in the time domain and the spectral amplitudes are linked. Also, since consecutive bursts result from consecutive collisions from alternating directions, the corresponding spectral components have the same spectral amplitude but differ in sign. This results in destructive spectral interference for even-order harmonics ($\omega=2m\omega_L$), while constructive interference occurs for odd harmonics [$\omega=(2m+1)\omega_L$].

However, if the symmetry is broken, even-order harmonics can be generated. The symmetry can be broken both on the level of the laser pulses and on the level of the medium properties. For laser pulse durations approaching the single-cycle regime (Brabec and Krausz, 2000), even-order harmonics can be generated near the cutoff until the high-energy part of the harmonic spectrum merges into a continuum (Spielmann *et al.*, 1997; Baltuška *et al.*, 2003). This results from a loss of the strict periodicity of electric-field oscillations within a laser pulse for pulse durations of less than 10 fs. In this case, the pulses consist of only a few optical cycles, breaking the symmetry between consecutive oscillations.

The inversion symmetry between the upper and lower half-cycles, which yields the spectrum of odd harmonics only, can also be broken by adding the second harmonic of the driving laser pulse (Mauritsson *et al.*, 2006). In this case, the shape and strength of the electric field in consecutive half-cycles differ beyond the simple sign change that occurs in a one color field, allowing for the production of attosecond pulse trains with only one pulse per infrared cycle with a stable carrier-envelope phase. For a one-color driver, there is a π phase flip from pulse to pulse in the harmonic attosecond pulse train. The addition of a weak second-harmonic field can also be exploited to generate single attosecond pulses in the multicycle-driver regime where usually multiple attosecond pulses are produced (Pfeifer *et al.*, 2006).

The same effect of creating a difference between consecutive half-cycles can be realized using oriented asymmetric molecules (Gavrilenko and Oks, 2000; Kreibich *et al.*, 2001). The anisotropy of such a medium makes the contributions from the upper and the lower half-cycle of the laser oscillations different (even for multicycle laser pulses), thus allowing the generation of even-order harmonics. Alignment (Stapelfeldt and Seideman, 2003) alone is not sufficient because the symmetry is not broken.

Due to the dependence of the harmonic phases on intensity, a blueshift of the harmonic peaks can occur. Since this effect is more pronounced for the longer trajectories because they spend more time in the electric field, the different amounts of blueshift between the different electron trajectories can even lead to a harmonic line splitting (Kan *et al.*, 1995).

C. Propagation and phase matching

The three-step model describes high-harmonic generation in the single-atom response by calculating atomic dipole moments from the electron dynamics, leading to the emission of a high-energy photon. It does not completely describe the harmonic-generation process in a medium. The discrete nature of the spectrum as presented in Sec. II.B is a result of the periodicity of the laser electric field. The final height and shape of the spectrum, however, are also determined by phase matching.

We now consider the various contributions to the phase mismatch in gases where conventional phase-matching techniques do not apply or are hard to implement. The wave vector k for a light wave transversing a gaseous medium can be written as follows (Rundquist *et al.*, 1998):

$$k = \underbrace{\frac{2\pi}{\lambda}}_{\text{vacuum term}} + \underbrace{\frac{2\pi N_a n(\lambda)}{\lambda}}_{\text{neutral gas}} \underbrace{- N_e r_e \lambda}_{\text{plasma dispersion}}, \tag{5}$$

where N_a is the density of neutral atoms in the medium (taking into account ionization losses), $n(\lambda)$ is the linear refractive index per unit neutral atom density (minus unity) at the wavelength λ, N_e is the density of free electrons, and r_e is the classical electron radius. The terms on the right-hand side of Eq. (5) represent the dispersion of the vacuum, the material, and the plasma. Note that the contribution from free electrons in the plasma is negative.

As we see later, it is advantageous to generate high-order harmonics in a gas-filled hollow fiber. Inside a hollow capillary, a superposition of fiber modes (Marcatili and Schmeltzer, 1964) is excited, making the pressure dependence of high-harmonic generation and the spatial beam profile of the generated radiation more complex. In general, the phase mismatch Δk between the generating laser field and the field of the high harmonics includes a dependence of the phase-mismatch $\Delta k = \Delta k(P, u_{nm})$ on the pressure P of the medium (the gas density) and the excited fiber modes u_{nm}.

In hollow fibers, we have another negative contribution given by the waveguide geometry, and the total wave vector can be written as

$$k = \frac{2\pi}{\lambda} + \frac{2\pi N_a n(\lambda)}{\lambda} - N_e r_e \lambda \underbrace{- \frac{u_{nm}^2 \lambda}{4\pi a^2}}_{\text{fiber dispersion}}, \tag{6}$$

where (in addition to the quantities defined above) u_{nm} is the mth root of the Bessel function $J_{n-1}(z)$ for the waveguide (for the lowest order, $u_{11}=2.405$), and a is the inner radius of the hollow fiber. Real and imaginary parts of the refractive index in the (soft-)x-ray region

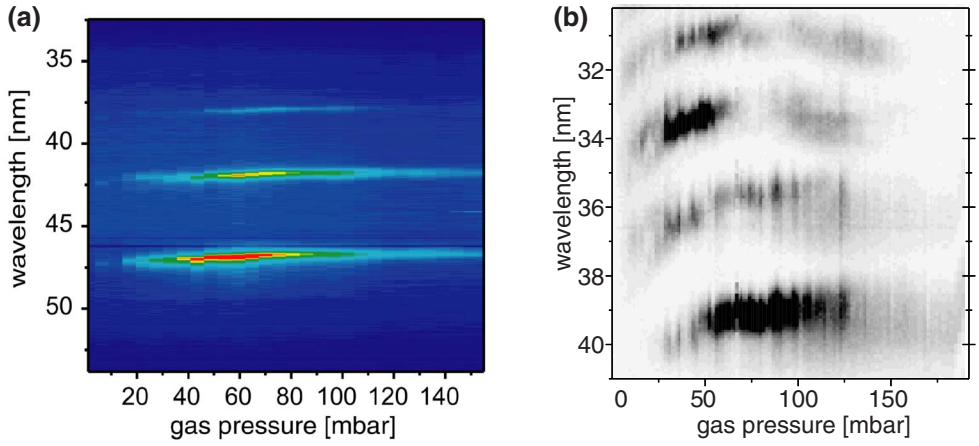

FIG. 4. (Color online) Pressure and mode dependence of high-harmonic generation in hollow fibers. (a) The excitation of one fiber mode shows the shift in maximum harmonic emission towards higher energies for increasing pressure. (b) If two different fiber modes are excited, two distinct local maxima can be seen. The maximum emission of 34 nm radiation at lower and higher pressure is governed by phase matching of the EH_{11} and EH_{12} fiber modes, respectively.

have been compiled by Henke *et al.* (1993).

In a phase-matched high-harmonic-generation process where the phase velocities of fundamental and harmonic beams are equal the phase mismatch for the qth harmonic order

$$\Delta k_q = q k_{\text{laser}} - k_{\text{x-ray}} \overset{!}{=} 0 \tag{7}$$

has to be equal to zero.

Substituting Eq. (6) into Eq. (7) and using $\lambda_{\text{x-ray}} = \lambda/q$ (where λ is the laser wavelength) we have

$$\Delta k_q = \frac{2\pi q}{\lambda}(1-\eta)P\Delta n - P\eta N_{\text{atm}} r_e \lambda \left[\frac{q^2-1}{q}\right] - \frac{u_{nm}^2 \lambda}{4\pi a^2}\left[\frac{q^2-1}{q}\right], \tag{8}$$

where we have introduced the pressure P (in atm), the ionization fraction η, the atomic number density at atmospheric pressure N_{atm}, and the difference between the refractive indices of the neutral gas at atmospheric pressure $\Delta n = n_{\text{laser}}^{\text{atm}} - n_{\text{x-ray}}^{\text{atm}}$. Since the highest harmonic conversion efficiency is obtained for $\Delta k = 0$ (phase matching), it is directly evident from Eq. (8) that there are several "control knobs" available.

(1) If we consider the case where only one fiber mode contributes to high-harmonic generation, there is still the possibility of adjusting the remaining parameters to achieve phase matching. It has been shown (Rundquist *et al.*, 1998; Durfee *et al.*, 1999) that the high-harmonic yield displays a maximum at a certain gas pressure P (neutral atom density), which corresponds to the phase-matched case $\Delta k = 0$ based on the pressure dependence of Δk. If we plot our experimental harmonic spectra versus the gas pressure in the capillary [Fig. 4(a)], we clearly see a shift of maximum harmonic emission towards higher frequencies for increasing pressure. Thus for a suitably chosen pressure, a certain range of harmonics is preferred.

(2) Since the highest harmonic conversion efficiency is obtained for $\Delta k = 0$ (phase matching), it is evident from Eq. (8) that there are several solutions of $\Delta k = 0$, one for each of the different fiber modes, i.e., different values of u_{nm}. Phase matching can therefore be achieved by exciting a suitable fiber mode which determines the value of u_{nm}. Experimentally, if more than one fiber mode is excited, we should see several local maxima in the pressure dependence of phase matching since the fiber-mode parameter u_{nm} assumes discrete values for different fiber modes. Figure 4(b) was recorded in a regime in which two fiber modes were excited by fundamental laser pulses. In this figure one can distinguish two separate local maxima of the harmonic yield as a function of the pressure. This experimental result matches well with theoretical calculation (Pfeifer, Kemmer, *et al.*, 2005) based on Eq. (8).

Another knob for dispersion control in a hollow-core fiber was proposed by Christov *et al.* (1998). By introducing thin glass plates with holes for the x-ray beam to pass into the waveguide, a periodic phase delay can be established for the fundamental, resulting in better phase matching.

If a fiber is not used for high-harmonic generation, but instead the driving laser is focused into the conversion medium, the Gouy phase $\eta(z)$ (Siegman, 1986) has to be taken into account. The geometric contribution to the wave vector by the hollow fiber has to be replaced by the contribution caused by the Gouy phase which depends on the Rayleigh range z_R (or equally on the confocal parameter b):

$$k_{\text{Gouy}} = \frac{d\eta(z)}{dz} = \frac{d}{dz}\arctan\left(\frac{z}{z_R}\right) \approx \frac{1}{z_R} \quad \left(=\frac{2}{b}\right), \tag{9}$$

where the last approximation is valid close to the focus ($z \ll z_R$). The additional phase mismatch originating from the Gouy phase shift undergone by a Gaussian beam across the focus is given as (Li *et al.*, 1989)

$$\Delta k_{\mathrm{Gouy}} = (q-1)\frac{2}{b}. \tag{10}$$

For very low gas densities, this term is actually the prevailing contribution to the total phase mismatch Δk (L'Huillier *et al.*, 1993). However, in the presence of strong ionization, the phase relationship is strongly perturbed (Bouhal *et al.*, 1998).

The contribution from the Gouy phase can be controlled by placing the focus at different positions with respect to the gas jet. This change in the phase-matching conditions allows the selection of the short or long electron quantum path in high-harmonic generation, influencing the spectral features of the emitted harmonic radiation (Salières *et al.*, 1995). The axial variation of the laser intensity leads to different phase-matching conditions for the contributions from different quantum paths. Depending on the geometry, ionization, and pressure conditions, phase matching can enhance one class of contributing trajectories at the expense of others: When the laser is focused before the generating medium, phase matching on the optical axis is efficient and the spatial and spectral harmonics are regular. For a focus at the center of the nonlinear medium, the harmonic yield is low due to poor phase matching. When the laser focus is positioned after the medium, efficient phase matching is only ensured for off-axis emission, leading to a high conversion efficiency but to distorted spatial and temporal profiles.

D. Attosecond pulse generation

One of the most promising aspects of high-harmonic generation is the ability to produce single pulses or pulse trains on the attosecond time scale. An early consideration by Farkas and Tóth (1992) showed that, similar to mode locking in a femtosecond oscillator (Siegman, 1986), high harmonics can be superimposed to yield attosecond pulses (with a duration of less than 100 as), provided a proper selection and phase relationship of the harmonics. The regular spacing of the harmonics in the spectral domain leads to the formation of attosecond pulse trains (Antoine *et al.*, 1996). Phase locking between five consecutive harmonics generated in argon was demonstrated by Paul *et al.* (2001). Isolated attosecond pulses with durations of 650 as could be generated by spectrally filtering the continuous cutoff region of few-cycle laser pulses (Hentschel *et al.*, 2001).

Consecutive experimental results have examined the existence of high-harmonic-based attosecond pulses and pulse trains in more detail (Mairesse *et al.*, 2003; Tzallas *et al.*, 2003) and have described successful first experiments where the unique properties of this new radiation can be exploited to follow electronic dynamics in real time (Drescher *et al.*, 2002; Kienberger *et al.*, 2002, 2004). A recent review on attosecond physics has been compiled by Agostini and DiMauro (2004) and Scrinzi *et al.* (2006). The time structure of single attosecond pulses and attosecond pulse trains depends on the so-called *femto chirp* and *atto chirp*, which has been discussed by Varjú *et al.* (2005).

E. Coherence

The first direct measurements of the temporal coherence of high-order harmonics were reported by Ditmire *et al.* (1996) and complemented by Bellini *et al.* (1998) and Lyngå *et al.* (1999). In the reported work, the authors measured the fringe visibility of the interference pattern in the far field of two spatially separated sources of harmonic radiation that were delayed in time with respect to each other. Whereas in general the coherence times are comparable to the expected pulse durations, the interference pattern exhibits two well-separated spatial regions (concentric rings) with significantly different coherence times for some harmonics: the intense inner part has a long coherence time while the outer region displays a much shorter coherence time. From the semiclassical interpretation of high-harmonic generation (Sec. II.A) there are actually two main trajectories that the electron can follow during the excursion time between ionization and recombination. The first (short) trajectory has a phase that does not vary much with laser intensity (Lewenstein *et al.*, 1995). Consequently, the emitted radiation has a long coherence time and is well collimated. The dipole phase of the second (long) trajectory, however, varies rapidly with laser intensity (Gaarde *et al.*, 1999), leading to a strong curvature of the phase front (due to the dependence of the intensity on the radial coordinate) and therefore to a strongly divergent angular emission (Salières *et al.*, 1995).

The spatial coherence of the high-harmonic light can be measured through the double-pinhole (or double-slit) interference technique. The modulation depth of the interference fringes after passing a beam through a pinhole pair is a direct measure for the degree of coherence across the spatial wave-front phase profile. If the phase difference between the two sampled points is constant, the fringe visibility will be unity whereas it is less than 1 if random phase variations exist. Bartels *et al.* (2002) used such a two-pinhole setup to verify full spatial coherence of high-harmonic radiation generated in a phase-matched hollow-fiber geometry (Rundquist *et al.*, 1998). From a classical viewpoint, high-harmonic generation driven by coherent light is an inherently coherent process. However, the degree of coherence is degraded by mechanisms such as plasma refraction and the time-varying index of refraction. Also, as mentioned above, at least two trajectories with different phase behavior contribute to high-harmonic generation. However, the quasiplane-wave interaction in a hollow fiber and the long propagation distance select a single trajectory, which improves both the temporal and the spatial coherence including the beam mode quality.

Measurements by Lee *et al.* (2003) confirmed the excellent spatial coherence of high-order harmonics from a gas-filled hollow fiber and used point-diffraction interferometry to show that the wave-front phase of a har-

monic beam can be considered as a spherical wave within a phase error of less than $\lambda/15$.

The first measurement of the spatial coherence of high-order harmonic radiation in the soft-x-ray region was performed by Ditmire *et al.* (1996). They executed a series of Young's two-slit experiments to find that the harmonics (generated in a gas plume) exhibit good fringe visibility and high spatial coherence. At high intensities the coherence is degraded due to the rapid production of free electrons, which imparts a rapidly varying phase on the harmonic, lowering the degree of coherence.

Based on the experiments by Bellini *et al.* (1998), Gaarde *et al.* (1999) presented a spatiotemporal analysis of high-harmonic radiation, demonstrating the separation into two quantum path components. Based on the numerical integration of the time-dependent Schrödinger equation, they determined the dipole moment $\mu_q(I)$ of the qth harmonic as a function of the intensity I of the laser field:

$$\mu_q(I) = A(I)\exp[i\Phi(I)]. \tag{11}$$

The dipole moment consists of several contributions with phases of the form

$$\Phi_k(r,z,t) = -\alpha_k I(r,z,t), \tag{12}$$

representing the different quantum paths, labeled by the index k. $I(r,z,t)$ is the space- and time-dependent intensity of the driving laser field, and α_k is the corresponding proportionality constant or slope of the phase function. By performing the equivalent of a time-frequency analysis using a window function for a range of intensities, the authors determined the "spectrum" of α_k. The result showed that the separation into different quantum path components is indeed justified. As representative values, they found the following numbers for α_k for the 15th harmonic in argon: $\alpha_1 \approx 1$ cm^2/W, $\alpha_2 \approx 27$ cm^2/W. The value for the long trajectory is much larger than for the short trajectory. Similar values are found in a study by Balcou *et al.* (1999). Gaarde (2001) calculated time-frequency representations of high-order harmonics for a more detailed analysis of the different chirps present.

The variation in time of the intensity $I(t)$ causes a frequency chirp $\Delta\omega_k(t) = -\partial\Phi_k(t)/\partial t$, leading to spectral broadening. Due to the time dependence of the intensity (Benedetti *et al.*, 2006) and the large value of α_k for the long trajectory, the radiation originating from this trajectory has a very short coherence time and a broad bandwidth since the harmonic pulse is strongly chirped.

In the same way, the radial variation of the intensity $I(r)$ introduces a curvature of the phase front, causing the beam to diverge, depending on the values of α and I. We can estimate the influence on both the curvature of the phase front and the chirp for both components. Using the values for α_k from above we find the ratios of the spectral widths $\Delta\omega_k$ and of the divergence angles θ_k (in a geometrical-optics approximation) as $\Delta\omega_2/\Delta\omega_1 \approx \theta_2/\theta_1 \approx 27$. Since the spectrum of the long trajectory is dominated by the dipole chirp whereas the spectral width of the short trajectory is determined by its Fourier-transform-limited broadening, this ratio reduces to values between 10 and 20 but is still very large for the two quantum paths.

Due to the spatially differing behavior (divergence angles) of radiation originating from the two trajectories, it is possible to macroscopically select only the short quantum path by placing an appropriate aperture in the harmonic beam, resulting in spatially and temporally highly coherent radiation. The separation of the two fields can also be achieved by introducing proper phase-matching conditions for the selection of one or the other contribution.

The atomic dipole phase [Eq. (12)] also depends on the harmonic order q. The α coefficients are closely related to the time the electrons spend in the continuum before recombination [return time or emission time (Mairesse *et al.*, 2003)] which is beyond the scope of this Colloquium.

F. Challenges and goals

The goal of femtosecond or attosecond time-resolved XUV or soft-x-ray spectroscopy poses several challenges as illustrated in Fig. 5. The upper left panel shows the starting situation of unoptimized high-harmonic spectra (Fig. 3). The other panels each feature one specific optimization goal: For instance, in order to be able to investigate the time-dependent shifts of absorption edges (Seres and Spielmann, 2007) the harmonic cutoff, which determines the highest energies possible, must be extended to shorter wavelengths (Spielmann *et al.*, 1998; Gibson *et al.*, 2003; Seres *et al.*, 2004, 2005); for any kind of nonlinear optics in the XUV range (Kobayashi, Ohno, *et al.*, 2000; Hentschel *et al.*, 2001; Papadogiannis *et al.*, 2003; Tzallas *et al.*, 2003; Miyamoto *et al.*, 2004; Sekikawa *et al.*, 2004; Hasegawa *et al.*, 2005); a large number of harmonic photons is desirable, therefore the efficiency of HHG should still be increased (Schnürer *et al.*, 1999) to make the whole range of methods of pump-probe technology available to the XUV domain; moreover, for both spectroscopic applications and the optimization of attosecond pulse durations (Mairesse *et al.*, 2003, 2004) the selection of single harmonics or ranges of consecutive harmonics is necessary.

In order to increase the count rates in photoelectron spectroscopy with high-harmonic radiation, a higher repetition rate of the harmonics is desirable. While it is very hard to increase the repetition rate of the driving laser due to limitations in the pump energies of the pump lasers in amplification stages, two groups (Gohle *et al.*, 2005; Jones *et al.*, 2005), have demonstrated high-harmonic generation directly from the oscillator. They succeeded in converting the frequency comb generated in a femtosecond oscillator cavity into the extreme ultraviolet (XUV) with intracavity high-harmonic generation at the full oscillator repetition rate by using an external buildup cavity with a xenon gas jet included in this cavity.

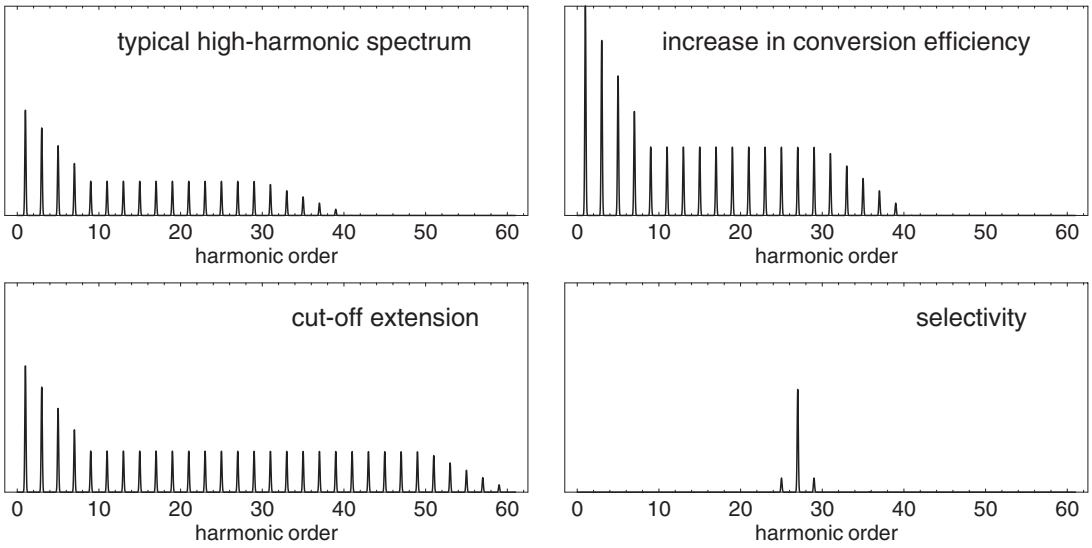

FIG. 5. Designed high-harmonic spectra to illustrate the challenges for further high-harmonic generation experiments: extension of the cutoff energy, increase in the efficiency of the high-harmonic conversion process, and the selection of single harmonics or range of harmonics.

In this work we concentrate on the generation of engineered coherent soft-x-ray spectra where harmonics can be selected or suppressed, based on adaptive temporal and spatial shaping of the driving fundamental laser pulses. We first discuss several recent experiments treated in the literature on this topic. Examples from our own research are then used to illustrate progress and possibilities in this field.

III. ADAPTIVE CONTROL

In order to shape high harmonics according to user-defined targets, it is convenient and effective to employ adaptive control schemes. This provides a powerful method to steer quantum-mechanical processes by applying an optimal light field (Brixner and Gerber, 2003). Numerous implementations in different areas have been reported in recent years, among others the control of chemical reactions (Assion *et al.*, 1998; Levis *et al.*, 2001), molecular population transfer (Bardeen *et al.*, 1997; Weinacht *et al.*, 1999; Brixner *et al.*, 2001; Herek *et al.*, 2002), atomic multiphoton absorption (Meshulach and Silberberg, 1998), and high-harmonic generation (Bartels *et al.*, 2000). The main experimental tool for achieving these goals is spectral phase shaping of femtosecond laser pulses (Weiner, 2000), in combination with evolutionary-algorithm-based experimental feedback loops (Judson and Rabitz, 1992; Baumert *et al.*, 1997; Yelin *et al.*, 1997).

Likewise, we expect soft-x-ray pulse shaping to be an efficient tool in our efforts towards the control of electronic motion. However, a direct transfer of pulse-shaping techniques developed in the optical wavelength range to the soft-x-ray regime is not feasible. Existing devices require either spectral dispersion [e.g., liquid-crystal (Weiner *et al.*, 1990) or acousto-optical (Fermann *et al.*, 1993) spatial light modulators or deformable mirrors (Zeek *et al.*, 1999)] or extensive passage through material [the acousto-optical programmable dispersive filter Dazzler (Verluise *et al.*, 2000)], which precludes their applicability in the soft-x-ray spectral range due to small diffraction efficiencies for spectral dispersion and high absorption coefficients. It appears more desirable to directly generate a shaped soft-x-ray pulse, for instance, by shaping the fundamental laser pulse prior to the conversion process than after its production. By shaping the ultrashort driving laser pulse it is possible to control the high-harmonic spectrum in a comprehensive way, far beyond earlier results on the control of particular spectral properties such as conversion efficiency and line width (Bartels *et al.*, 2000, 2001) or the blueshift of harmonics (Reitze *et al.*, 2004).

Due to the temporally coherent nature of the soft-x-ray light generated by high-harmonic generation, spectral shaping and engineering, on the other hand, means the ability to shape the emerging trains of attosecond pulses or single attosecond pulses. These results open the possibility towards adaptive control in the soft-x-ray spectral range.

Based on the complete Hamiltonian, the potential energy surfaces and the dynamics of a quantum system can be calculated theoretically. In principle, the control of this quantum system is possible by applying the correct electric field (e.g., of a laser). The great difficulty is to determine the exact electric field that is needed to steer a quantum-mechanical reaction towards the desired output. Derived from simple resonance problems, researchers tried to selectively break a chemical bond by tuning the incident light field to the vibrational frequency of the selected bond. However, other than was expected, in most cases the weakest bond broke due to intramolecular vibrational energy redistribution (IVR). The vibrational energy coupled into the system by the light field quickly redistributes over the whole system through the

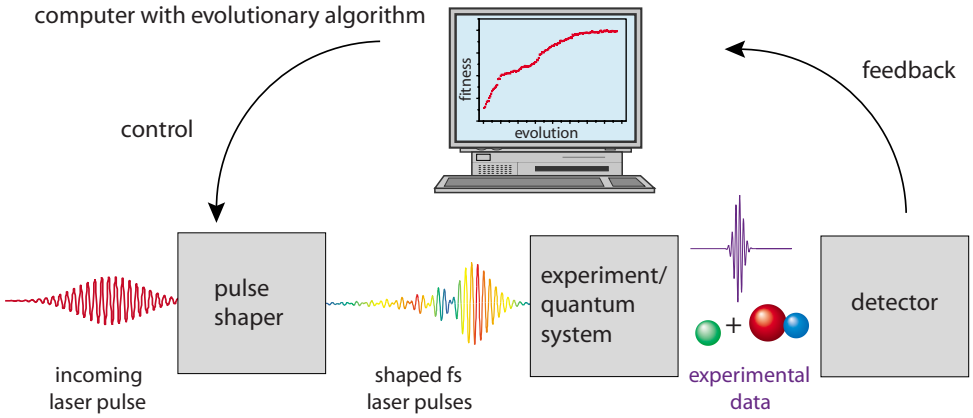

FIG. 6. (Color online) Working principle of adaptive control. The incoming laser pulse is first shaped in a laser pulse shaper and is then used to perform the experiment in the quantum system. The experimental signal is analyzed and a fitness is assigned to the corresponding laser pulse. Utilizing this ranking, the evolutionary algorithm can automatically and iteratively find the optimum laser pulse shape.

coupling of the vibrational modes. A more complex electric field is therefore required to exactly cleave a desired chemical bond.

The problem of finding this electric field can be solved by applying different pulse shapes in a closed-loop optimization setup as proposed by Judson and Rabitz (1992), which we also employed for the adaptive control of high-harmonic generation in this work. Laser pulses are automatically tailored in a temporal or spatial pulse shaper according to user-defined optimization goals.

The basic working principle is depicted in Fig. 6. It relies on an evolutionary algorithm (Baumert *et al.*, 1997) that finds an optimal electric field. In brief, the incoming laser pulses are shaped in some sort of pulse shaper. The modulated laser pulses (in Fig. 6 a temporally shaped laser pulse is shown) are then used to perform the experiment in the quantum system. The experimental signal is analyzed and a fitness is assigned to the corresponding laser pulse. Utilizing this ranking, the evolutionary algorithm can automatically find the optimum laser pulse. The first experimental implementations by Yelin *et al.* (1997) and Baumert *et al.* (1997) automatically compressed chirped femtosecond laser pulses, without first characterizing the pulses.

In our setups to shape the high-harmonic spectra, the closed-loop optimization iteratively shapes the laser pulse either temporally with a deformable mirror (Sec. IV) or spatially using a two-dimensional liquid-crystal-display-based spatial light modulator (Sec. V). The obtained spectrum is measured with a charge coupled device (CCD) camera. The applied algorithm is based on the evolutionary principle of "survival of the fittest" (Baumert *et al.*, 1997). A fitness measure for each shaped laser pulse is derived from the high-harmonic spectrum. This measure, also termed fitness function, maps the shape of the complete high-harmonic spectrum onto a single number. In this way it is possible to rank the performance of different laser pulse shapes according to how well it produced the desired harmonic spectrum or spectral feature. Each pulse shape termed an individual is characterized by a number of genes, e.g., the 19 high-voltage levels applied to the deformable mirror electrodes. These voltage parameters defining the pulse shape can therefore be regarded as the genetic elements of an individual laser pulse. Fifty different individuals represent a generation. The first generation consists of individuals each possessing randomly chosen genes (voltages) with values throughout the suitable voltage range. After applying those pulses in the harmonic generation experiment, their fitness is determined and the selection of the fittest is carried out. The evolutionary algorithm uses the ranking by the fitness function to keep the best-performing laser pulses for the next generation. The rest is dismissed or transferred to the next generation by mutation (some genetic elements are randomly changed) or crossover (two individuals of the old generation each pass on a part of their genetic elements to their "offspring") until a population size of fifty is reached again. The members of the new generation are now tested for their performance in order to build the following generation, and the closed-loop optimization iteratively converges towards a maximum fitness value by gradually improving the laser pulse shapes from one generation to the next.

IV. CONTROL OF HIGH-HARMONIC GENERATION THROUGH TEMPORAL LASER PULSE SHAPING

Control of high-harmonic radiation should be possible in two fundamental ways, either by controlling the temporal evolution of the driving electric field or by controlling spatial properties in the broadest sense, including medium engineering and geometric effects. The temporal aspect are described in this section while spatial aspects can be found in Sec. V.

The temporal evolution of the electric field $\boldsymbol{E}(t)$ of an ultrashort laser pulse can be summarized as

$$\boldsymbol{E}(t) = E_{\mathrm{env}}(t)\boldsymbol{p}(t)e^{i[\omega t+\varphi(t)+\varphi_0]}, \tag{13}$$

where $E_{\mathrm{env}}(t)$ is the envelope of the pulse effectively determining the pulse duration and pulse intensity, $\boldsymbol{p}(t)$ is the polarization axis which can vary during the duration of the pulse, ω is the central frequency and can be modified, e.g., in multicolor experiments, $\varphi(t)$ is the time-varying phase and determines the chirp of the laser pulse, and φ_0 is the carrier-envelope phase which we have written here explicitly since it plays an important role for few-cycle laser pulses and the generation of single attosecond pulses.

Here we describe a number of experiments that systematically adjusted one of these parameters manually in order to control high-harmonic radiation. This is also called open-loop control since no feedback from the experiment is used to close the optimization loop. As the number of possible configurations is extremely high, it is very convenient to use an evolutionary algorithm as presented in Sec. III to quickly find an optimum setting.

A. Open-loop control

Several attempts have been made to influence harmonic spectra and the corresponding harmonic light pulses. As explained in Sec. II, the same intense laser field is responsible for the ionization of the medium and the subsequent acceleration of electrons so that they can gain kinetic energy. In order to replace the initial effective multiphoton ionization by a linear single-photon step and to have control over the initial phase of the electron with respect to the accelerating laser field, it was first proposed and calculated by Schafer *et al.* (2004) and experimentally verified by the group of Ursula Keller (Biegert *et al.*, 2006) to separate these two steps. First, a regularly spaced attosecond pulse train (APT) consisting of high-photon-energy harmonic pulses is generated in a hollow fiber filled with xenon gas. This attosecond pulse train is then directed into a helium gas jet, together with a strong fundamental laser pulse. The high-energy photon from the APT can now ionize the gas efficiently in a direct one-photon transition while the second fundamental laser field is responsible for the acceleration of the electron. The timing between these two fields can be controlled, allowing for quantum-path selection on the single-atom level, decoupling the ionization step from the strong-field dynamics.

Another implication of the fact that usually the same laser field is employed for the ionization and acceleration of electrons is the limit that is placed on the highest obtainable photon energy (cutoff energy). The actual laser intensity I in Eq. (1) has to be substituted by the saturation intensity I_s (Chang *et al.*, 1997; Schnuerer *et al.*, 1998), which atoms can be exposed to before saturation is reached, i.e., before the number of atoms left available in the neutral ground state has become negligible. For high-intensity pulses with long pulse durations (multicycle pulses), the medium is depleted before the high peak intensity is reached since the number of ionized atoms increases in a stepwise fashion at each maximum of the oscillations of the electric field, leaving no neutral atoms to be ionized and available for high-harmonic generation at the highest intensities. The cutoff therefore appears at lower harmonic orders than what is expected from the laser pulse peak intensity in Eq. (3). This limit can be circumvented for very short driving pulses (few-cycle or single-cycle pulses) since in this case the high peak intensity of the envelope nearly coincides with the first peak of the oscillatory electric field. A sizable number of electrons are born into a very strong electric field and can acquire higher kinetic energies than before when the ground state was depleted before the peak of the envelope had been reached. The cutoff energy no longer depends on the intensity of the laser pulse alone, but on the pulse duration as well [Chang *et al.*, 1997, Eq. (2)]. This dependence was used by Chang *et al.* (1997, 26 fs pulses) Schnürer *et al.* (1998, sub-10-fs pulses) to extend high-harmonic generation into the water window (4.4–2.3 nm) where water absorbs less than carbon (Spielmann *et al.*, 1997; Chang *et al.*, 1998b) and is therefore of high interest to time-resolved soft-x-ray spectroscopy of biological samples.

Lee *et al.* (2001) have shown that the high-harmonic generation process can be controlled coherently using chirped femtosecond laser pulses to produce sharp and strong harmonic spectra. For an efficient coherent control, a proper laser chirp condition must be chosen to suppress the harmonic chirp that broadens high harmonics and reduces their peak intensities. This chirp depends on the current laser intensity used. Chang *et al.* (1998a) have demonstrated theoretically and experimentally that for positively chirped pump pulses (precompensation of the harmonic chirp), the individual harmonic peaks are well defined and discrete, while for negatively chirped pump pulses (additional contribution to the negative harmonic chirp), the harmonic output spectra merge into a continuum. Adjusting the laser chirp and/or energy also allows for continuous wavelength tuning of the high-order harmonics, covering the entire spectral region between two consecutive harmonics (Altucci *et al.*, 1999; Kim *et al.*, 2003).

A detailed analysis (Mauritsson *et al.*, 2004) including a cross correlation of the generated harmonics and a theoretical calculation (Murakami *et al.*, 2005) showed that a chirp on the pump pulse generating the harmonics is transferred to the qth harmonic as q times the fundamental chirp, verifying an earlier analysis by Chang *et al.* (1998a). For bandwidth-limited pulses, the harmonics are negatively chirped due to the atomic dipole phase, so by adding a positive chirp on the pump pulse, the harmonic chirp can be compensated.

Lopez-Martens *et al.* (2005) demonstrated amplitude and phase control of attosecond light pulses by introducing a thin aluminum filter in the beam path of the harmonic pulses. High-harmonic pulses are intrinsically chirped due to the intensity dependence of the atomic phase [phase accumulated during excursion on the quantum paths (Lewenstein *et al.*, 1995; Salières *et al.*, 2001)]. For the short quantum path which can be selected by placing a hard aperture in the fundamental laser beam

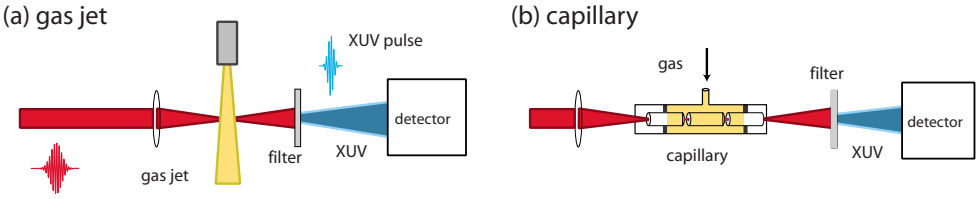

FIG. 7. (Color online) Geometries for high-harmonic generation in atomic or molecular gaseous media. (a) Generation in a free-focusing geometry (gas jet), selectivity of single harmonics is not possible. (b) Generation inside a gas-filled hollow capillary, selectivity of different single harmonics can be achieved with a high contrast with respect to neighboring orders.

prior to harmonic generation this chirp is positive. This results in temporally long harmonic pulses. This phase can be compensated by the negative material dispersion introduced by the aluminum filter in the XUV wavelength range. A train of almost Fourier-transform-limited pulses with pulse durations of 170 as can be obtained, characterized with RABBITT (Muller, 2002; Mairesse *et al.*, 2003; López-Martens *et al.*, 2004). The same group (Mairesse *et al.*, 2003) proposed to use a plasma compressor for the synchronization of high harmonic since the free electrons in a plasma also induce the required negative group velocity dispersion. The use of material dispersion was suggested by Kim *et al.* (2004) to obtain single sub-50 as pulses. The use of extreme-ultraviolet chirped mirrors has also been proposed as a way to compress attosecond harmonic pulses (Morlens *et al.*, 2005).

Another way to control high-harmonic generation is by controlling the time-dependent polarization state of the electric field during the driving laser pulse duration. The process of high-harmonic generation is sensitive to the ellipticity of the driving light field (Weihe and Bucksbaum, 1996; Flettner, König, *et al.*, 2003). Only for linear polarization can the electron return to its parent ion to recombine and emit harmonic photons. A time-varying polarization can be realized by combining two short perpendicularly polarized pulses with slightly different center frequencies (Corkum *et al.*, 1994; Ivanov *et al.*, 1995), by polarization gating using two waveplates or other birefringent optics (Altucci *et al.*, 1998; Strelkov *et al.*, 2004; Zair *et al.*, 2004), or by direct polarization pulse shaping of the fundamental driving laser field (Oron *et al.*, 2005) using a polarization pulse shaper. Polarization pulse shaping has been introduced by Brixner and Gerber (2001) and has been demonstrated, e.g., for the two-photon ionization of potassium dimers (Brixner *et al.*, 2004). Calculations (Chang, 2005) have shown that the chirp of a single attosecond pulse generated by polarization gating is positive and its value is almost the same as that when a linearly polarized laser is used. Using polarization gating and phase stabilized pulses (Sola *et al.*, 2006) it was possible to generate single-cycle isolated attosecond pulses around 36 eV (Sansone *et al.*, 2006) Applying a complete temporal characterization technique the estimated pulse duration was as low as 130 as, representing the shortest man-made electromagnetic pulses so far.

B. Tailoring high-harmonic spectra by adaptive temporal pulse shaping (closed-loop control)

In addition to the open-loop results reported above, the implementation of a closed-loop scheme represents a very powerful method to comprehensively shape high-harmonic spectra, beyond the extent possible by simply modeling the high-harmonic generation process.

1. Adaptive optimizations in gas jets

There are two main geometries that can be employed to generate high harmonics in a gas target: generation in a gas jet or in a hollow gas-filled capillary (Fig. 7). A simple setup consists of the intense laser pulses being focused into a gas jet as shown in Fig. 7(a). The XUV radiation produced in the gas jet by the highly nonlinear interaction of laser pulses with gas atoms is separated from the fundamental field by a suitable filter, e.g., by a thin 300 nm aluminum filter for harmonics in the energy range from 20 to 70 eV and is subsequently detected by a soft-x-ray spectrometer.

Earlier experiments performed in gas jets successfully tuned the harmonic wavelengths via blueshift (Reitze *et al.*, 2004). The 27th harmonic at 30 nm could be shifted to 31.16 nm. The authors attribute this shift to ionization effects. They also attempted to enhance single harmonics relative to adjacent peaks. However, the selective control of single harmonics using such a free-focusing geometry has not been achieved so far. Also our result in Fig. 8(a) shows that it is impossible to enhance a single harmonic in a gas jet (yield in region A compared to the yield in regions B).

On the other hand, it is possible to extend the cutoff in a free-focusing geometry [Fig. 8(b)], using the deformable mirror as described in Sec. IV. The optimization of the cutoff position in HHG is due to the clean-up of higher-order phase distortions by the deformable mirror, thus increasing the laser peak intensity, leading to higher cutoff photon energies. An enhanced level of control including the selectivity of selected harmonic orders can only be achieved in a waveguide geometry such as a hollow fiber.

There has also been a theoretical study on the optimization of high-harmonic generation in noble gases using a genetic algorithm (Roos *et al.*, 2001). Harmonic radiation could be tailored to different applications such as optimization of the pulse energy of one harmonic, mini-

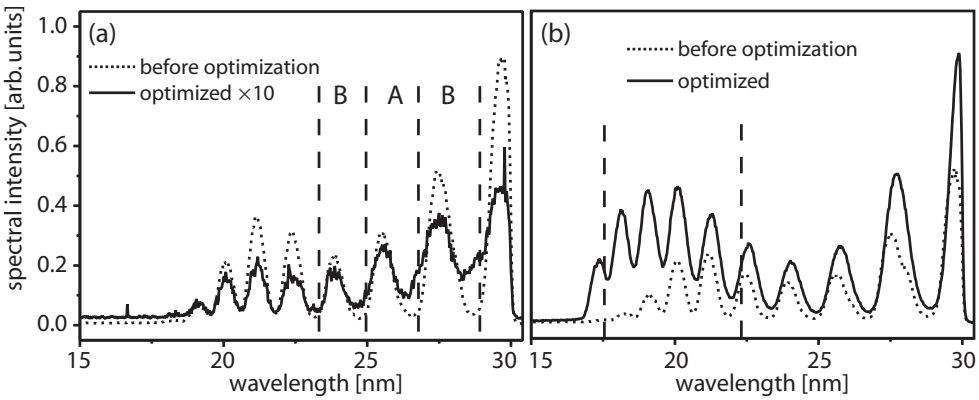

FIG. 8. Optimizations of harmonics performed in a free-focusing geometry. (a) Negative outcome of a selective optimization of harmonics in region A compared to region B. No selectivity could be achieved. (b) Cutoff extension in a free-focusing geometry. The optimization of the high-harmonic cutoff position is due to the clean-up of higher-order phase distortions by the deformable mirror, thus increasing the laser peak intensity, leading to higher cutoff photon energies.

mization of the pulse duration, and the optimization of the temporal coherence of harmonics. This was done by adaptively adjusting the intensity of the laser, the gas pressure, the interaction length in the nonlinear medium, and the position of the focus relative to the gas jet.

Another theoretical investigation (Yedder *et al.*, 2004) used an efficient genetic algorithm to optimize short intense excitation laser pulses in order to generate high-order harmonics from which single attosecond pulses can be synthesized. Whereas the high-harmonic field generated by an unoptimized laser pulse exhibits the well-known train structure (Antoine *et al.*, 1996) with a number of satellites, single attosecond pulses appear after the optimization.

2. Enhanced control in hollow fibers

A capillary setup where the laser is focused into a hollow fiber filled with a noble gas [Fig. 7(b)] allows for selective enhancement (Bartels *et al.*, 2000, 2001; Pfeifer, Walter, *et al.*, 2005). Earlier work (Bartels *et al.*, 2000) demonstrated the optimization of a single harmonic generated in an argon-filled hollow fiber. This was achieved using spectral-phase shaping with a micromachined deformable mirror. Additional work by the same group (Bartels *et al.*, 2001) showed the enhancement of different harmonic orders in different noble gases, although the contrast ratio between the selected harmonic and neighboring harmonics is lower.

Going far beyond these earlier results we demonstrate the complete control over the XUV spectrum of high harmonics. We achieved both the enhancement and suppression of high-harmonic emission in a selected wavelength region as well as the enhancement of coherent soft-x-ray radiation over a selectable extended range of harmonics. In order to find the laser pulse shapes that are needed to exert this level of control we employed an evolutionary algorithm.

The experimental setup used for these experiments is displayed in Fig. 9: Ultrashort laser pulses from a regeneratively amplified Ti:sapphire laser system (80-fs pulse duration, 800-nm center wavelength, 0.8-mJ pulse energy, 1-kHz repetition rate) are spectrally broadened in an argon-filled hollow fiber (250-μm inner diameter, 0.6-m length, 0.6-bar pressure) by the process of self-phase modulation (Nisoli *et al.*, 1996). Using a prism compressor with a deformable mirror as a retroreflector (Pfeifer *et al.*, 2003), we are able to obtain 20-fs pulses that can be phase shaped by controlling the surface of the deformable mirror. The shaped pulses are focused into a second argon-filled fiber with an inner diameter of 140 μm and a length of 0.1 m. This fiber is split into three parts which are aligned on a V-groove mount with tiny gaps between them to ensure a constant pressure in the center segment where high-harmonic generation takes place. The outer segments serve as a seal towards the vacuum before and after the fiber. The laser intensity inside the capillary can be estimated as 2×10^{14} W/cm^2 from the cutoff scaling law. After a 0.3-μm-thick aluminum filter which blocks the fundamental and lower orders the harmonic radiation is detected with a soft-x-ray CCD camera mounted behind a grazing-incidence XUV spectrometer. Rundquist *et al.* (1998) used a similar setup to demonstrate phase-matched generation of high harmonics in a hollow capillary. They were able to increase the harmonic output by two to three orders of magnitude compared to the non-phase-matched case. Similar values were reported by Tamaki *et al.* (1999). Spatial effects inside a fiber such as phase matching are discussed in Sec. V.

Control over the high-harmonic spectrum is achieved by employing an evolutionary algorithm (Baumert *et al.*, 1997). This algorithm drives the gold membrane of the deformable mirror (inset of Fig. 9) to shape the laser pulses by sending specific voltage values to electrodes behind the gold membrane. The gold membrane is deformed depending on the applied voltage and thus changes the optical path of the individual wavelength components of the laser pulse that are spatially dispersed in a prism compressor. The high-harmonic spectra generated by these shaped pulses are recorded by the

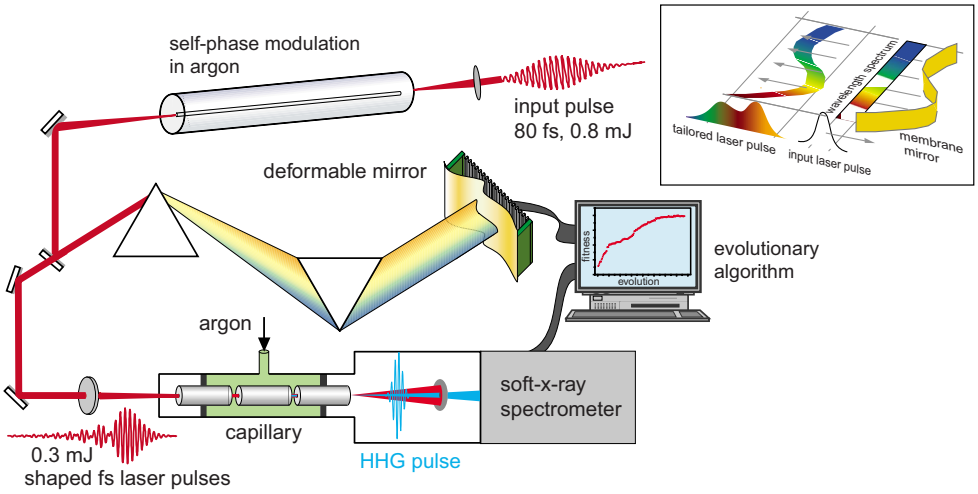

FIG. 9. (Color online) Experimental setup for temporal pulse shaping. Ultrashort laser pulses from a regenerative amplifier undergo further spectral broadening and compression using self-phase modulation in an argon-filled hollow capillary and a prism compressor. A deformable mirror as the symmetry plane of the prism compressor allows temporal pulse shaping. The shaped pulses generate high-harmonic radiation in a second argon-filled hollow fiber. The resulting spectrum is recorded by a CCD camera equipped soft-x-ray spectrometer and analyzed by the computer which runs a closed-loop evolutionary algorithm to optimize the spectral shape. The upper inset depicts the modification of the optical paths of the different frequency components as introduced by the deformable mirror. The inset on the right shows a typical optimization run for the selection of a single harmonic. The fitness value increases as a function of the number of generations.

CCD camera that evaluates them according to a given fitness function. The closed-loop optimization iteratively converges towards a maximum fitness value by gradually improving the laser pulse shapes.

We can now follow our goals defined above and try to selectively generate single harmonics or a range of harmonics. We are able to enhance a particular harmonic order while simultaneously keeping neighboring orders at low intensity (Fig. 10). The fitness function in this case was defined as the spectrally integrated yield of the target harmonic divided by the integrated yield of the other harmonic orders. Compared to previous measurements (Bartels *et al.*, 2000, 2001) our results show an unprecedented contrast ratio between the selected harmonic

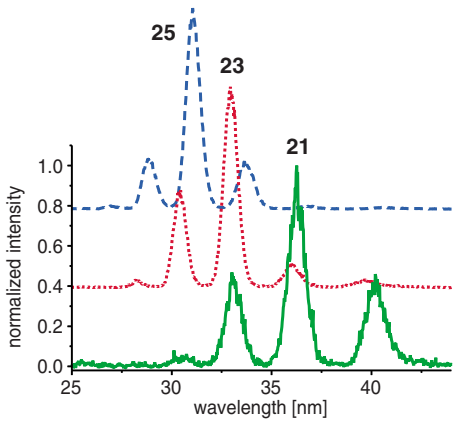

FIG. 10. (Color online) Optimizations of different single harmonic orders in a hollow fiber. Harmonics can be selected with a high contrast ratio with respect to neighboring orders.

and suppressed neighboring orders. Direct neighbors of the optimized harmonic order are relatively weak while there is a negligible contribution from all others. These tunable quasimonochromatic high-harmonic spectra allow for time-resolved spectroscopy in the soft-x-ray region.

A comparison between the two experiments on the optimization of high harmonics in a gas jet and in a capillary [Figs. 8(a) and 10] reveals that an enhancement of single harmonics in a free-focusing geometry such as a gas jet is not possible. The results by Reitze *et al.* (2004) confirm this finding. This contradicts the explanation given by Bartels *et al.* (Bartels *et al.*, 2000, 2001; Christov *et al.*, 2001) which is based on the single-atom response only and does not include propagation effects. Instead, comparison shows that a spatial contribution arising from the mode distribution in a hollow fiber is essential to the optimization. The results of our investigation of spatial effects in a capillary are summarized in Sec. V.

We also succeeded at the selection of a certain range of consecutive harmonic orders. Figure 11(b) shows the optimization of the long-wavelength spectral part while simultaneously reducing the short-wavelength region and vice versa [Fig. 11(c)]. Considering the reduced peak intensity in a temporally shaped and thus chirped generating laser pulse, the selective generation of lower orders can be understood since the cutoff is shifted towards lower energies. However, it remains unclear what process is responsible for the enhancement of higher orders while at the same time lower orders are suppressed almost completely.

Another example of our ability to control the generated harmonic spectra is displayed in Fig. 12. The upper

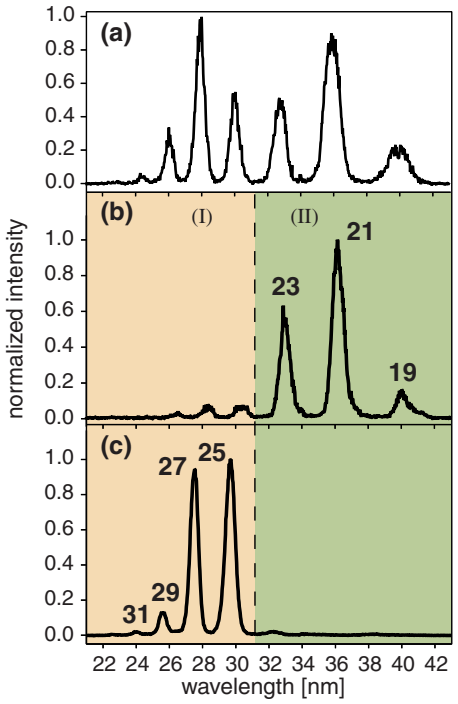

FIG. 11. (Color online) Selection of extended frequency ranges of high-harmonic orders. (a) Reference spectrum obtained with an unmodulated laser pulse. (b) Optimization of the long-wavelength spectral part while simultaneously reducing the short-wavelength region and (c) vice versa.

part shows a typical harmonic spectrum in the plateau region while the lower part demonstrates the suppression of one and two harmonics, respectively. The unshaped spectrum reveals a maximum due to phase matching inside the capillary. However, the harmonics are nearly equally intense, implying that the displayed range lies in the plateau region. To our knowledge this is the first demonstration of the suppression of single plateau harmonics. Complete control over the shape of the soft-x-ray spectrum has a major impact on ultrafast energy-resolved spectroscopy and on the temporal structure of high harmonics. Section VI discusses some of the implications on the attosecond time structure of generated radiation. The following section examines the spatial properties of high-harmonic generation in a hollow fiber and considers propagation effects such as phase matching.

V. CONTROL OF HIGH-HARMONIC GENERATION THROUGH SPATIAL ENGINEERING

Up to now only the temporal shaping of high-harmonic radiation in a hollow fiber has been considered. However, Figs. 8 and 10 imply that spatial effects determined by the waveguide geometry have to be taken into account in order to obtain a high level of control over the harmonics as demonstrated above. However, control of the spatially coherent nature of the process is essential for maximizing the yield.

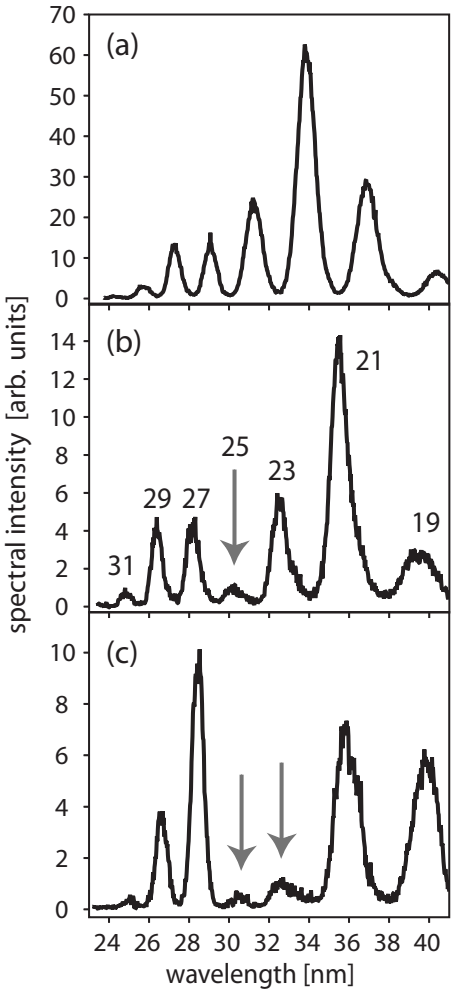

FIG. 12. Suppression of harmonics. (a) Starting with a typical harmonic spectrum in the plateau region, we can suppress (b) one or (c) two harmonic orders. These modifications of the spectra imply major modulations of the harmonic time structure on an attosecond time scale.

A. Free-focusing geometry

Work done on controlling the spatial shape of generating laser pulses by use of a two-dimensional deformable mirror has been able to enhance only the overall conversion efficiency in a jet geometry by cleaning up higher-order spatial phase distortions (Yoshitomi *et al.*, 2003; Villoresi *et al.*, 2004). Their result closely resembles our result in Fig. 8, which shows a similar effect. Note, however, that the cutoff extension in our experiments was mainly achieved by cleaning up the temporal profile of the laser pulse while higher-order spatial phase distortions are corrected in the work by Villoresi *et al.* (2004).

Kazamias *et al.* (2002) and Sutherland *et al.* (2004) reported marked enhancements in high-harmonic generation in a gas cell filled with noble gases when a partially closed aperture is placed in the path of the laser beam before the focusing lens (truncation). They attributed this effect to the effective *f*-number, the laser beam spatial quality, and the interplay between the laser phase

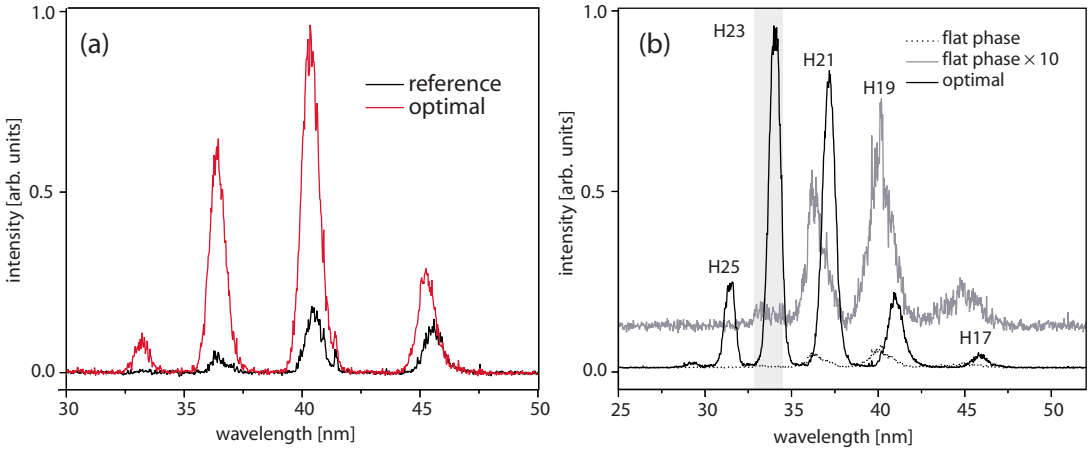

FIG. 13. (Color online) Optimization of high-harmonic emission in a hollow fiber using spatial laser pulse shaping. (a) Optimization of the total yield results in an increase by a factor of 5. (b) Selective enhancement of the 23rd harmonic (gray-shaded area) as the optimization goal results in an increase by two orders of magnitude. However, no selectivity is achieved.

and the intrinsic phase of the harmonics. Apparently, the aperture introduces phase variations on the laser wave front that minimize the phase mismatch. Here we demonstrate the importance of spatial effects in achieving full control over the process of high-harmonic generation.

B. Fiber-mode excitation

As we have seen in Sec. II.C, several fiber modes can contribute to high-harmonic generation in a hollow fiber, opening different phase-matching windows (Fig. 4). Which fiber modes are excited after the driving laser has been coupled into the fiber can be adjusted by modifying the spatial amplitude and phase profile of the driving laser pulse at the entrance of the fiber. However, the systematic selection of specific fiber modes is impossible due to the mode-coupling effect. Near the critical power of self-focusing inside the fiber different fiber modes no longer travel independently as linearly independent modes but start to mix (Tempea and Brabec, 1998; Homoelle and Gaeta, 2000). This effect is responsible for a changing mode distribution as a function of propagation along the fiber. Therefore we need an optimization algorithm that is able to manipulate the spatial properties of the driving laser pulse to fulfill the phase-matching condition inside the fiber exactly at the harmonic generation point.

To examine the influence of excitation of different fiber modes on the process of high-harmonic generation more thoroughly, a two-dimensional spatial pulse shaper for the fundamental laser pulses was set up in order to modify their spatial phase before they are coupled into the fiber. By shaping the spatial phase of the laser pulse before focusing, we are able to control the amplitude and phase profile of the pulse in its Fourier plane located at the entrance of the capillary.

This pulse shaper is based on a computer-controlled electrically addressable phase-only spatial light modulator by Hamamatsu Photonics (programmable phase modulator PPM X8267). An adjustable phase between 0 and 2π can be added to the local spatial phase of the laser pulse separately for each pixel (Kobayashi, Igasaki, *et al.*, 2000). The shaped laser pulses excite different modes in the fiber used for high-harmonic generation. The harmonic spectra are recorded by a CCD camera. An evolutionary algorithm is used to run the closed-loop optimization of certain optimization goals.

In order to test the abilities of this setup to excite arbitrary fiber modes as needed for the spatial optimization of high-harmonic generation we used a helium-neon laser focused into a similar fiber. The fiber output is recorded by a CCD camera to evaluate the excited fiber modes. The fitness function is defined as the integral overlap between the recorded picture and a predefined bitmap mask representing the desired fiber modes. We were thus able to selectively excite the fundamental mode, double and triple modes, as well as ring modes or random patterns, demonstrating the capability of our setup for the adaptive spatial control of fiber modes and their excitation for high-harmonic generation (Walter *et al.*, 2006).

C. Optimizations in a hollow-core fiber

The optimization of the high harmonics based on selective fiber mode excitation should now be possible. Our first approach is to enhance the total harmonic yield beyond the value that can be achieved by manually optimizing the coupling of the laser into the fiber. After the adaptive optimization, the total yield increases by approximately a factor of 5 [Fig. 13(a)]. We also tried to selectively enhance a single harmonic order as was done in the case of temporal pulse shaping (Sec. IV). The result is shown in Fig. 13(b) where the shaded area marks the wavelength range over which the yield of the selected harmonic is integrated, squared, and divided by the integrated yield of the neighboring orders to define the fitness function (gas pressure: 170 mbar). As can be seen, the yield of the selected cutoff harmonic increases

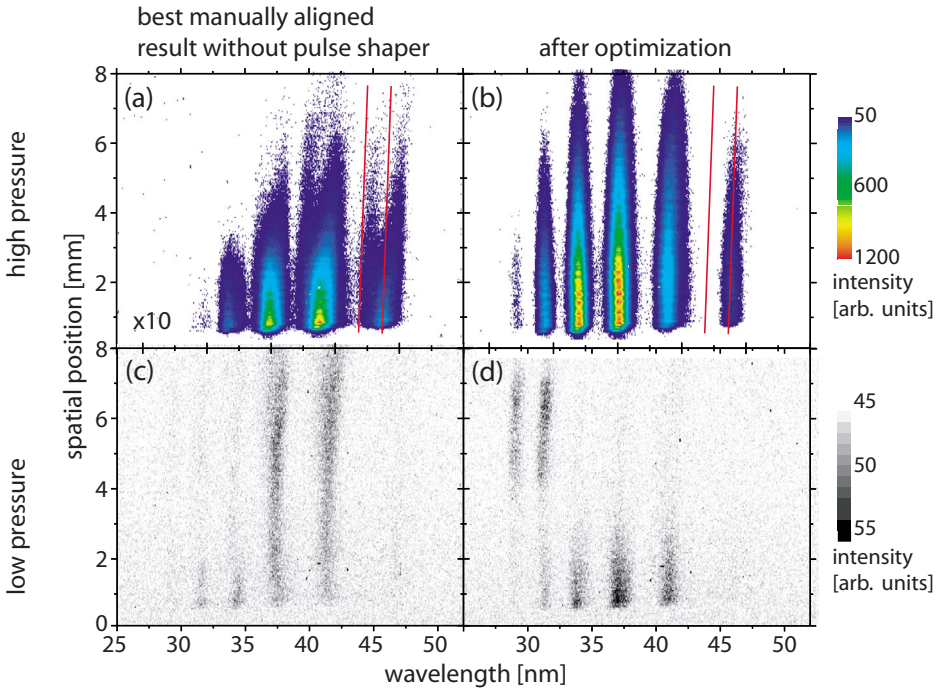

FIG. 14. (Color online) Spatially resolved HHG spectra: (a), (b) high pressure and (c), (d) low pressure. Two fiber modes contribute to the signal in (a) before the optimization while the optimized pulse (b) results in an overall increase in intensity of about ten. The excitation of a single mode is clearly visible. At low pressures the change in excited fiber modes from (c) before the optimization to (d) after the optimization becomes more evident.

by more than two orders of magnitude. Obviously spatial optimization of high-harmonic radiation is possible. However, the contrast ratio between the selected single harmonic and the neighboring orders is not nearly as high as in the case of temporal phase shaping (Fig. 10). This implies the necessity to use temporal and spatial pulse shaping in order to selectively enhance single harmonics.

The calculation of the expected harmonic mode profiles based on the initial spatial phase of the laser pulse is very difficult. Due to the high intensities that are present in the fiber, ionization of the conversion medium occurs and leads to significant distortions of the propagating laser pulse inside the fiber. The initially excited fiber mode distribution changes constantly due to this nonlinear mode coupling (Jenkins and Devereux, 1992). It is therefore important to excite a single fiber mode at the point inside the capillary where the harmonics are predominantly generated (center piece in our setup). Not only is it very difficult to calculate the initial spatial intensity and phase profile needed, but it is almost impossible to reproduce exactly the calculated profile experimentally. This again explains why a closed-loop optimization based on an evolutionary algorithm is of great value.

The excitation of different fiber modes can be made visible by spatially resolving the harmonic beam along the spectrometer slit [Figs. 14(a) and 14(b)]. Before optimization [Fig. 14(a)], each harmonic is split up into two contributions at two distinct center wavelengths. The two contributions originate from two fiber modes. Since the transverse intensity distribution within the fiber and thus the degree of ionization varies for different fiber modes, this results in different amounts of blueshift. After the optimization [Fig. 14(b)] with the goal to enhance the 23rd harmonic order the bimodal structure inherent to Fig. 14(a) disappears, leaving a clear single-mode harmonic spectrum.

Enhancement of the selected harmonic order could be due to better phase matching based on the selection of a suitable fiber mode that can fulfill Eq. (8). An increased intensity inside the fiber due to an improvement of the coupling into the fiber as a reason for the observed enhancement can be ruled out. In this case, the amount of blueshift should have increased whereas in our measurement there is less blueshift after the optimization. Furthermore, if the single-atom response was responsible for the enhancement, an increased intensity would have led to the production of higher harmonic orders, which is not the case. By decreasing the pressure in the fiber from 170 to 20 mbars we are no longer in the phase-matching regime, thereby switching off the effective mode filter caused by phase matching. Nonlinear mode-coupling effects also become negligible as a consequence that spatial changes in the generating pulse directly carry over to the harmonic beam. Figures 14(c) and 14(d) show substantial differences in the beam shape between neighboring harmonic orders for the unoptimized as well as for the optimized case. This indicates the contribution from different fiber modes during the generation of high harmonics.

D. Optimizing the geometry: Quasi-phase-matched generation

Using a modulated hollow-core waveguide (Paul *et al.*, 2003) instead of a hollow capillary with flat walls in order to periodically vary the intensity of the laser light driving the conversion, high harmonics can be generated at significantly higher photon energies, even in the presence of substantial ionization. Higher levels of ionization, caused by the higher intensity of the driving laser

to extend the cutoff, normally cause the phase velocity of the pump beam to be too fast to be phase matched.

Quasi-phase-matching (QPM), originally proposed by Armstrong *et al.* (1962), introduces an additional term $K=2\pi/\Lambda$ into the phase-matching expression (8), where Λ is the modulation period. A periodicity corresponding to twice the coherence length corrects the phase mismatch and allows for more efficient nonlinear frequency conversion. In the modulated waveguide the intensity of the laser is reduced in regions where the harmonic light is out of phase by 180° with the driving laser (after one coherence length) by expanding the diameter of the waveguide so that no new harmonics are generated. This pattern is repeated periodically for a full quasi-phase-matching scheme. Decreasing the modulation period of the walls of the waveguide (Gibson *et al.*, 2003), coherent light can even be generated in the water window using gas-filled hollow fibers.

A different method to achieve a periodically varying generation efficiency for nonlinear frequency upconversion can be realized by density modulations of the medium to modulate the nonlinear susceptibility (Shkolnikov *et al.*, 1996).

E. Optimizing the medium

Since harmonic generation is a coherent process, the resulting harmonic electric field scales linearly with the particles density of the interacting medium, leading to a quadratic dependence of the intensity. However, for the cutoff harmonics, a maximum density is given by the ionization-induced defocusing of the laser pulse (Altucci *et al.*, 1996). Instead of using gas targets, we made the transition from gaseous to liquid targets and investigated water microdroplets as a source of high-harmonic radiation (Flettner, Pfeifer, *et al.*, 2003). We studied the emission of XUV radiation from water microdroplets under excitation with either a single or a pair of intense femtosecond laser pulses. Varying the delay between the two pulses we observed a transition from pure incoherent plasma emission to coherent high-harmonic generation. Under optimized conditions we obtained high-harmonic radiation up to the 27th order.

High-harmonic generation in a dense medium such as water microdroplet also was the subject of a theoretical study by Strelkov *et al.* (2005). The three-dimensional Schrödinger equation was solved for a single-electron atom in the combined fields of the neighboring particles and the laser and the results were averaged using a Monte Carlo method. Since the long and the short trajectory are affected differently by the random variation of the harmonic phase in the presence of the medium, sharper harmonic lines and shorter attosecond pulses can appear due to the suppression of the long path. At very high densities, harmonic lines are compressed completely. Also, electrons can possibly be captured by neighboring ions. However, due to the random distribution of particles in the medium no coherent emission occurs for these electrons. Hence there is no extension of the single-atom cutoff.

A different approach to overcome low particle densities is to increase the interaction length. This can be done by focusing the intense laser pulses into a gas-filled hollow capillary (Marcatili and Schmeltzer, 1964; Davies and Mendonça, 2000) instead of a short gas jet. In combination with the negative dispersion of the hollow fiber the variation of the gas pressure inside the fiber provides an additional control parameter to compensate the phase mismatch between the fundamental wave and the generated harmonic. This results in a notable increase of the conversion efficiency (Rundquist *et al.*, 1998; Durfee *et al.*, 1999; Paul *et al.*, 2003). The use of hollow fibers has already been discussed in the previous sections of this work.

Proper phase matching can also be ensured in a gas cell (Delfin *et al.*, 1999; Tamaki *et al.*, 2000) where the laser is loosely focused, provided the correct placement of the focus with respect to the entrance of the gas cell. Kazamias, Douillet, Valentin, *et al.* (2003) and Kazamias, Douillet, Weihe, *et al.* (2003) used the analysis of the coherence length for constructive harmonic buildup based on Maker fringes (Maker *et al.*, 1962) to optimize the conversion efficiency.

In addition to controlling the electric field that drives high-harmonic generation, the nonlinear medium itself can be engineered. Apart from atomic gases, high harmonics can be generated in simple (Liang *et al.*, 1997) and complex molecules (Fraser *et al.*, 1995; Hay *et al.*, 2000; Altucci *et al.*, 2006), clusters (Donnelly *et al.*, 1996), or solid surfaces (Norreys *et al.*, 1996) (although the generation mechanism is different for the latter).

If a molecule is stretched out well beyond its equilibrium distance by preparing a highly excited vibrational state, harmonic peaks of much higher energies in units of the ponderomotive energy than those predicted for a single atom or ground-state molecule can be detected (Moreno *et al.*, 1997). According to this numerical simulation, the large internuclear separation allows the electron to be detached from one of the cores, but recombine with the partner core. A similar behavior with kinetic energies reaching $8U_p$ has been found by Lein (2005). By using a two-color excitation in extended molecular systems, harmonics at energies of $6U_p$ to $10U_p$ can be generated (Bandrauk *et al.*, 1997). A high-frequency prepulse ensures sufficient ionized electrons, while a second lower-frequency pulse accelerates them towards the other atom in the stretched molecule. Also, controlling the ground-state wave function of the electron in a stretched molecule can increase the efficiency of high-harmonic generation (Pfeifer *et al.*, 2004). Since the electronic wave function is more delocalized for a stretched molecule as compared to a ground-state molecule, it experiences less spreading during continuum propagation, increasing the probability of recombination of the returning electron with the parent ion.

VI. HIGH-HARMONIC TIME STRUCTURE

The results on temporal and spatial shaping presented above demonstrate our capabilities to generate arbitrary

high-harmonic spectra. However, the question of the time structure of our shaped harmonics as generated in a hollow capillary remains open.

Proper selection of harmonics generated in a gas jet enables pulse durations in the attosecond regime (Hentschel *et al.*, 2001; Paul *et al.*, 2001; Mairesse *et al.*, 2003). The controlled selection of range of harmonic orders is essential to the optimization of attosecond pulses. According to the work by Mairesse *et al.* (2003), selecting a larger and larger region of harmonics does not necessarily lead to shorter (attosecond) pulses. More harmonics result in more spectral width, but since the harmonics are intrinsically chirped the harmonic pulse duration may effectively increase in spite of the broadened spectrum. The chirp results from the different excursion times of electrons generating the different harmonic orders. In order to produce the shortest attosecond pulse possible, the appropriate number of harmonics with suitable relative phases has to be chosen, which can now be done using our pulse shaping technique. This circumvents the problem of finding a suitable filter that can select the desired range. Also, the conventional selection with a grating is accompanied with a loss of time resolution due to dispersion and with a substantial reduction in photon number and is thus not desirable. Besides providing a superior way of selecting specific high-harmonic frequencies our approach also allows for shifting the range of harmonics and consequently for tuning the wavelength of the resulting attosecond pulses or attosecond pulse trains.

Most of the previously published experiments used bandwidth-limited laser pulses or laser pulses with a controlled linear chirp and high-harmonic generation was done in a gas jet. On the other hand, during our optimization of harmonic generation in a gas-filled hollow fiber, the spectral phase of the driving laser pulses is adapted continuously according to the fitness in order to reach the predefined optimization goal. This in turn modifies the harmonic phase. In addition, there are propagation effects inside the relatively long fiber compared to the focus in a gas jet or gas cell. Therefore the pulse duration of such a single adaptively selected harmonic order is completely unknown. The knowledge is crucial for spectroscopic applications since conventional filtering using gratings is accompanied with a loss in time resolution due to dispersion and a significant decrease in photon number. Therefore work is in progress to determine the time structure of our adaptively shaped harmonics using a cross-correlation setup.

Currently there is much interest in the generation of attosecond pulses. In addition to characterization experiments cited above, there are efforts to actively control the phase of high harmonics in order to get rid of its inherent wavelength dependence to produce bandwidth-limited attosecond pulses. This can be achieved using aluminum filters that have a negative dispersion in the desired energy range (López-Martens *et al.*, 2005) or by designing XUV chirped mirrors (Morlens *et al.*, 2005).

A recent theoretical study (Xiao *et al.*, 2006) showed that by optimizing the chirp and initial phase of the driving laser pulses with the help of a genetic algorithm, the peak intensity of single attosecond pulses can be enhanced by one or two orders of magnitude. In addition, the pulse duration is automatically greatly compressed and the optimal propagation distance determined.

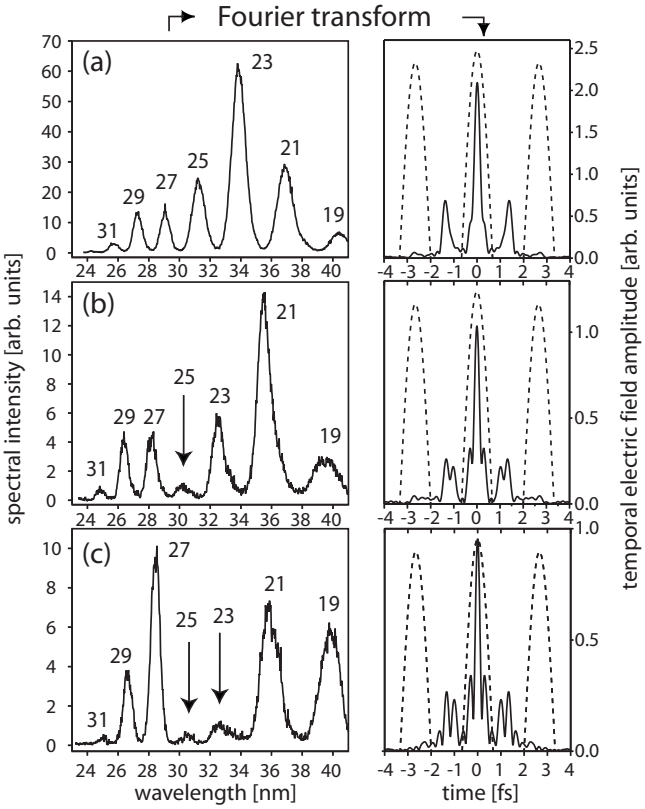

FIG. 15. High-harmonic spectra and their corresponding Fourier transform assuming a flat spectra phase. (a) The unshaped spectrum show the periodicity of $T/2$ for the harmonic pulses in the time domain as expected. (b) One or (c) two suppressed harmonics result in an increased effective spacing of frequency components and thus in a sub-half-cycle modulation of the harmonic time structure.

Our ability to shape the spectrum of high-harmonic pulses as demonstrated in Secs. IV and V enables us to modify the time structure of high harmonics on an attosecond time scale. Figure 15 (left column) displays shaped harmonic spectra where one or two orders have been suppressed. The right column of Fig. 15 represents the corresponding Fourier transforms of these spectra, assuming a flat phase. Of course, the assumption is not valid since harmonics are known to have a remaining linear chirp. In addition, our shaped harmonics must have additional contributions from the chirp of the driving laser pulse since at least part of it is transferred to the harmonics in the fiber. However, this calculation shows interesting features caused by the suppression of one or two harmonics. Since in addition to the harmonic spacing of 2ω there is another spacing of more than 2ω between the harmonic contributions on the left and on the right of the suppressed orders, there must be a modulation in the time domain of less than half a laser period. The dotted line in Fig. 15 shows the envelope of

the electric field with a period of T so that harmonics are generated with a period of $T/2$. This results in the harmonic spacing of $2\pi/(T/2)=2\omega$. Since the spacing in the frequency domain is effectively larger in the presence of the suppressed orders, the period of the harmonics in the time domain is smaller than $T/2$, which means that there is a sub-half-cycle or attosecond modulation. Even though the assumption of a flat spectral phase is not correct, these results are qualitatively valid and show the attosecond modifications of the harmonic pulses caused by adaptively shaping them using the pulse shaper. This consideration demonstrates the potential of our technique for extending pulse shaping into the attosecond regime. Adaptive quantum control of electron dynamics in the gas phase and condensed phase is therefore possible.

VII. CONCLUSION

In conclusion, we have summarized recent developments and achievements in the field of optimal control of high-harmonic generation. Depending on the geometry of the setup and on the type of control (open loop, adaptive feedback loop, temporal shaping, spatial shaping), different levels of tailoring high-harmonic spectra and high-harmonic pulses are possible. The efficiency of the frequency conversion process can be improved, and the position and/or shape of the resulting harmonic peaks can be influenced.

We have demonstrated that the use of a hollow-fiber setup allows for the generation of arbitrarily shaped high-harmonic spectra, including both the enhancement and the suppression of single or several selected harmonic orders. Both temporal pulse shaping and spatial propagation effects are necessary in order to selectively enhance single harmonics with a high contrast ratio. The manipulation of discrete harmonic peaks results in attosecond modifications of the attosecond pulse train generated by these harmonics. However, shifting our technique towards the continuum part of the cutoff region will represent an attosecond pulse shaper for true isolated attosecond pulses.

Tailored harmonic spectra are of current interest and importance for the field of frequency or time-resolved spectroscopy in the XUV and soft-x-ray regions of the spectrum. A number of applications have demonstrated the power and versatility of this laboratory-scale tabletop light source for probing matter properties both in the spectral and in the temporal domain, in an energy range and with a time resolution previously inaccessible. However, up to now none of them employed adaptive shaping of high-harmonic radiation as demonstrated in this work to extend the capabilites and the usefullness of this radiation. Applications that could greatly benefit from these developments include the following: EUV microscopy and submicron imaging, time-resolved photoemission spectroscopy of surface chemistry, and time-resolved measurements of electronic dynamics such as the Auger decay and innershell lifetimes in atoms and solids. The possibility to shape high harmonics greatly extends the field of applications and broadens the level of information retrieved from such measurements.

Future work on the optimal control of high-harmonic generation will include a combination of temporal and spatial pulse shaping to investigate the physical background in more detail. Furthermore, since we have shown that shaping the harmonic radiation in the spectral domain allows for modifications of the time structure on an attosecond time scale, this constitutes the first steps towards building an attosecond pulse shaper in the soft-x-ray domain.

ACKNOWLEDGMENTS

We would like to thank the following people for their contribution: Ron Kemmer, Alexander Paulus, Thomas Pfeifer, Robert Spitzenpfeil, and Dominik Walter. This work was supported by the Deutsche Forschungsgemeinschaft (Grant No. SP 687/1-3), the Austrian Science Fund (Grant No. F016), the German-Israeli Cooperation in Ultrafast Laser Technologies, and the Fonds der Chemischen Industrie. One of the authors (C.W.) acknowledges support from the Studienstiftung des deutschen Volkes.

REFERENCES

Agostini, P., and L. F. DiMauro, 2004, Rep. Prog. Phys. **67**, 813.
Agostini, P., F. Fabre, G. Mainfray, G. Petite, and N. K. Rahman, 1979, Phys. Rev. Lett. **42**, 1127.
Altucci, C., R. Bruzzese, C. de Lisio, M. Nisoli, S. Stagira, S. De Silvestri, O. Svelto, A. Boscolo, P. Ceccherini, L. Poletto, G. Tondello, and P. Villoresi, 1999, Phys. Rev. A **61**, 021801(R).
Altucci, C., C. Delfin, L. Roos, M. B. Gaarde, A. L'Huillier, I. Mercer, T. Starczewski, and C.-G. Wahlström, 1998, Phys. Rev. A **58**, 3934.
Altucci, C., T. Starczewski, E. Mevel, and C.-G. Wahlström, 1996, J. Opt. Soc. Am. B **13**, 148.
Altucci, C., R. Velotta, E. Heesel, E. Springate, J. P. Marangos, C. Vozzi, E. Benedetti, F. Calegari, G. Sansone, S. Stagira, M. Nisoli, and V. Tosa, 2006, Phys. Rev. A **73**, 043411.
Ammosov, M. V., N. B. Delone, and V. P. Krainov, 1986, Sov. Phys. JETP **64**, 1191.
Andruszkow, J., *et al.*, 2000, Phys. Rev. Lett. **85**, 3825.
Antoine, P., A. L'Huillier, and M. Lewenstein, 1996, Phys. Rev. Lett. **77**, 1234.
Armstrong, J. A., N. Bloembergen, J. Ducuing, and P. S. Pershan, 1962, Phys. Rev. **127**, 1918.
Assion, A., T. Baumert, M. Bergt, T. Brixner, B. Kiefer, V. Seyfried, M. Strehle, and G. Gerber, 1998, Science **282**, 919.
Ayvazyan, V., *et al.*, 2006, Eur. Phys. J. D **37**, 297.
Balcou, P., A. S. Dederichs, M. B. Gaarde, and A. L'Huillier, 1999, J. Phys. B **32**, 2973.
Baltuška, A., T. Udem, M. Uiberacker, M. Hentschel, E. Goulielmakis, C. Gohle, R. Holzwarth, V. S. Yakovlev, A. Scrinzi, T. W. Hänsch, and F. Krausz, 2003, Nature (London) **421**, 611.
Bandrauk, A. D., S. Chelkowski, H. Yu, and E. Constant, 1997, Phys. Rev. A **56**, R2537.
Bardeen, C. J., V. V. Yakovlev, K. R. Wilson, S. D. Carpenter, P. M. Weber, and W. S. Warren, 1997, Chem. Phys. Lett. **280**, 151.

Bartels, R., S. Backus, I. Christov, H. Kapteyn, and M. Murnane, 2001, Chem. Phys. **267**, 277.
Bartels, R., S. Backus, E. Zeek, L. Misoguti, G. Vdovin, I. P. Christov, M. M. Murnane, and H. C. Kapteyn, 2000, Nature (London) **406**, 164.
Bartels, R. A., A. Paul, H. Green, H. C. Kapteyn, M. M. Murnane, S. Backus, I. P. Christov, Y. W. Liu, D. Attwood, and C. Jacobsen, 2002, Science **297**, 376.
Baumert, T., T. Brixner, V. Seyfried, M. Strehle, and G. Gerber, 1997, Appl. Phys. B: Lasers Opt. **65**, 779.
Baumert, T., M. Grosser, R. Thalweiser, and G. Gerber, 1991, Phys. Rev. Lett. **67**, 3753.
Bellini, M., C. Lyngå, A. Tozzi, M. B. Gaarde, T. W. Hänsch, A. L'Huillier, and C.-G. Wahlström, 1998, Phys. Rev. Lett. **81**, 297.
Benedetti, E., J.-P. Caumes, G. Sansone, S. Stagira, C. Vozzi, and M. Nisoli, 2006, Opt. Express **14**, 2242.
Biegert, J., A. Heinrich, C. P. Hauri, W. Kornelis, P. Schlup, M. P. Anscombe, M. B. Gaarde, K. J. Schafer, and U. Keller, 2006, J. Mod. Opt. **53**, 87.
Bloembergen, N., 1999, Rev. Mod. Phys. **71**, S283.
Bouhal, A., P. Salières, P. Breger, P. Agostini, G. Hamoniaux, A. Mysyrowicz, A. Antonetti, R. Constantinescu, and H. G. Muller, 1998, Phys. Rev. A **58**, 389.
Brabec, T., and F. Krausz, 2000, Rev. Mod. Phys. **72**, 545.
Brixner, T., N. H. Damrauer, P. Niklaus, and G. Gerber, 2001, Nature (London) **414**, 57.
Brixner, T., and G. Gerber, 2001, Opt. Lett. **26**, 557.
Brixner, T., and G. Gerber, 2003, ChemPhysChem **4**, 418.
Brixner, T., G. Krampert, T. Pfeifer, R. Selle, G. Gerber, M. Wollenhaupt, O. Graefe, C. Horn, D. Liese, and T. Baumert, 2004, Phys. Rev. Lett. **92**, 208301.
Chang, Z., 2005, Phys. Rev. A **71**, 023813.
Chang, Z., A. Rundquist, H. Wang, I. Christov, H. C. Kapteyn, and M. M. Murnane, 1998a, Phys. Rev. A **58**, R30.
Chang, Z., A. Rundquist, H. Wang, I. Christov, M. M. Murnane, and H. C. Kapteyn, 1998b, IEEE J. Sel. Top. Quantum Electron. **4**, 266.
Chang, Z., A. Rundquist, H. Wang, M. M. Murnane, and H. C. Kapteyn, 1997, Phys. Rev. Lett. **79**, 2967.
Christov, I. P., R. Bartels, H. C. Kapteyn, and M. M. Murnane, 2001, Phys. Rev. Lett. **86**, 5458.
Christov, I. P., H. C. Kapteyn, and M. M. Murnane, 1998, Opt. Express **3**, 360.
Christov, I. P., M. M. Murnane, and H. C. Kapteyn, 1997, Phys. Rev. Lett. **78**, 1251.
Corkum, P. B., 1993, Phys. Rev. Lett. **71**, 1994.
Corkum, P. B., N. H. Burnett, and M. Y. Ivanov, 1994, Opt. Lett. **19**, 1870.
Daido, H., 2002, Rep. Prog. Phys. **65**, 1513.
Davies, J. R., and J. T. Mendonça, 2000, Phys. Rev. E **62**, 7168.
Delfin, C., C. Altucci, F. De Filippo, C. de Lisio, M. B. Gaarde, A. L'Huillier, L. Roos, and C.-G. Wahlström, 1999, J. Phys. B **32**, 5397.
Ditmire, T., J. K. Crane, H. Nguyen, L. B. DaSilva, and M. D. Perry, 1995, Phys. Rev. A **51**, R902.
Ditmire, T., E. T. Gumbrell, R. A. Smith, J. W. G. Tisch, D. D. Meyerhofer, and M. H. R. Hutchinson, 1996, Phys. Rev. Lett. **77**, 4756.
Donnelly, T. D., T. Ditmire, K. Neuman, M. D. Perry, and R. W. Falcone, 1996, Phys. Rev. Lett. **76**, 2472.
Dorner, R., H. Schmidt-Bocking, T. Weber, T. Jahnke, M. Schoffler, A. Knapp, M. Hattas, A. Czasch, L. P. H. Schmidt, and O. Jagutzki, 2004, Radiat. Phys. Chem. **70**, 191.
Drescher, M., M. Hentschel, R. Kienberger, G. Tempea, C. Spielmann, G. A. Reider, P. B. Corkum, and F. Krausz, 2001, Science **291**, 1923.
Drescher, M., M. Hentschel, R. Kienberger, M. Uiberacker, V. Yakovlev, A. Scrinzi, T. Westerwalbesloh, U. Kleineberg, U. Heinzmann, and F. Krausz, 2002, Nature (London) **419**, 803.
Durfee, C. G., III, A. Rundquist, S. Backus, C. Herne, M. M. Murnane, and H. C. Kapteyn, 1999, Phys. Rev. Lett. **83**, 2187.
Farkas, G., and C. Tóth, 1992, Phys. Lett. A **168**, 447.
Fermann, M. E., V. da Silva, D. A. Smith, Y. Silberberg, and A. M. Weiner, 1993, Opt. Lett. **18**, 1505.
Fittinghoff, D. N., P. R. Bolton, B. Chang, and K. C. Kulander, 1992, Phys. Rev. Lett. **69**, 2642.
Flettner, A., J. König, M. B. Mason, T. Pfeifer, U. Weichmann, and G. Gerber, 2003, J. Mod. Opt. **50**, 529.
Flettner, A., T. Pfeifer, D. Walter, C. Winterfeldt, C. Spielmann, and G. Gerber, 2003, Appl. Phys. B: Lasers Opt. **77**, 747.
Franken, P. A., A. E. Hill, C. W. Peters, and G. Weinreich, 1961, Phys. Rev. Lett. **7**, 118.
Fraser, D. J., M. H. R. Hutchinson, J. P. Marangos, Y. L. Shao, J. W. G. Tisch, and M. Castillejo, 1995, J. Phys. B **28**, L739.
Freeman, R. R., P. H. Bucksbaum, H. Milchberg, S. Darack, D. Schumacher, and M. E. Geusic, 1987, Phys. Rev. Lett. **59**, 1092.
Gaarde, M. B., 2001, Opt. Express **8**, 529.
Gaarde, M. B., F. Salin, E. Constant, P. Balcou, K. J. Schafer, K. C. Kulander, and A. L'Huillier, 1999, Phys. Rev. A **59**, 1367.
Gavrilenko, V. P., and E. Oks, 2000, J. Phys. B **33**, 1629.
Gibson, E. A., A. Paul, N. Wagner, R. Tobey, D. Gaudiosi, S. Backus, I. P. Christov, A. Aquila, E. M. Gullikson, D. T. Attwood, M. M. Murnane, and H. C. Kapteyn, 2003, Science **302**, 95.
Giulietti, D., and L. A. Gizzi, 1998, Riv. Nuovo Cimento **21**, 1.
Gohle, C., T. Udem, M. Herrmann, J. Rauschenberger, R. Holzwarth, H. A. Schuessler, F. Krausz, and T. W. Hänsch, 2005, Nature (London) **436**, 234.
Hasegawa, H., E. J. Takahashi, Y. Nabekawa, K. L. Ishikawa, and K. Midorikawa, 2005, Phys. Rev. A **71**, 023407.
Hay, N., M. Castillejo, R. de Nalda, E. Springate, R. J. Mendham, and J. P. Marengos, 2000, Phys. Rev. A **61**, 053810.
Henke, B. L., E. M. Gullikson, and J. C. Davis, 1993, At. Data Nucl. Data Tables **54**, 181.
Hentschel, M., R. Kienberger, C. Spielmann, G. A. Reider, N. Milosevic, T. Brabec, P. Corkum, U. Heinzmann, M. Drescher, and F. Krausz, 2001, Nature (London) **414**, 509.
Herek, J. L., W. Wohlleben, R. J. Cogdell, D. Zeidler, and M. Motzkus, 2002, Nature (London) **417**, 533.
Homoelle, D., and A. L. Gaeta, 2000, Opt. Lett. **25**, 761.
Ivanov, M., P. B. Corkum, T. Zuo, and A. Bandrauk, 1995, Phys. Rev. Lett. **74**, 2933.
Jenkins, R. M., and R. W. J. Devereux, 1992, Appl. Opt. **31**, 5086.
Jones, R. J., K. D. Moll, M. J. Thorpe, and J. Ye, 2005, Phys. Rev. Lett. **94**, 193201.
Judson, R. S., and H. Rabitz, 1992, Phys. Rev. Lett. **68**, 1500.
Kan, C., C. E. Capjack, R. Rankin, and N. H. Burnett, 1995, Phys. Rev. A **52**, R4336.
Kazamias, S., D. Douillet, C. Valentin, F. Weihe, F. Augé, T. Lefrou, G. Grillon, S. Sebban, and P. Balcou, 2003, Phys. Rev. A **68**, 033819.

Kazamias, S., D. Douillet, F. Weihe, C. Valentin, A. Rousse, S. Sebban, G. G. F. Augé, D. Hulin, and P. Balcou, 2003, Phys. Rev. Lett. **90**, 193901.
Kazamias, S., F. Weihe, D. Douillet, C. Valentin, T. Planchon, S. Sebban, G. Grillon, F. Augé, D. Hulin, and P. Balcou, 2002, Eur. Phys. J. D **21**, 353.
Keitel, C. H., and P. L. Knight, 1995, Phys. Rev. A **51**, 1420.
Keldysh, L. V., 1965, Sov. Phys. JETP **20**, 1307.
Kienberger, R., E. Goulielmakis, M. Uiberacker, A. Baltuška, V. Yakovlev, F. Bammer, A. Scrinzi, T. Westerwalbesloh, U. Kleineberg, U. Heinzmann, M. Drescher, and F. Krausz, 2004, Nature (London) **427**, 817.
Kienberger, R., M. Hentschel, M. Uiberacker, C. Spielmann, M. Kitzler, A. Scrinzi, M. Wieland, T. Westerwalbesloh, U. Kleineberg, U. Heinzmann, M. Drescher, and F. Krausz, 2002, Science **297**, 1144.
Kim, H. T., D. G. Lee, K. H. Hong, J. H. Kim, I. W. Choi, and C. H. Nam, 2003, Phys. Rev. A **67**, 051801.
Kim, K. T., C. M. Kim, M.-G. Baik, G. Umesh, and C. H. Nam, 2004, Phys. Rev. A **69**, 051805(R).
Kobayashi, Y., Y. Igasaki, N. Yoshida, N. Fukuchi, H. Toyoda, T. Hara, and M. H. Wu, 2000, Proc. SPIE **3951**, 158.
Kobayashi, Y., T. Ohno, T. Sekikawa, Y. Nabekawa, and S. Watanabe, 2000, Appl. Phys. B: Lasers Opt. **70**, 389.
Kreibich, T., M. Lein, V. Engel, and E. K. U. Gross, 2001, Phys. Rev. Lett. **87**, 103901.
Kulander, K. C., K. J. Schafer, and J. L. Krause, 1993, in *Super-Intense Laser-Atom Physics*, edited by B. Piraux, A. L'Huillier, and K. Rzazewski, NATO Advanced Studies Institute No. 316, Series B: Physics (Plenum, New York), p. 95.
Lee, D. G., J. H. Kim, K. H. Hong, and C. H. Nam, 2001, Phys. Rev. Lett. **87**, 243902.
Lee, D. G., J. J. Park, J. H. Sung, and C. H. Nam, 2003, Opt. Lett. **28**, 480.
Lein, M., 2005, Phys. Rev. A **72**, 053816.
Levis, R. J., G. Menkir, and H. Rabitz, 2001, Science **292**, 709.
Lewenstein, M., P. Balcou, M. Y. Ivanov, A. L'Huillier, and P. B. Corkum, 1994, Phys. Rev. A **49**, 2117.
Lewenstein, M., P. Salières, and A. L'Huillier, 1995, Phys. Rev. A **52**, 4747.
L'Huillier, A., and P. Balcou, 1993, Phys. Rev. Lett. **70**, 774.
L'Huillier, A., M. Lewenstein, P. Saliéres, P. Balcou, M. Y. Ivanov, J. Larsson, and C. G. Wahlström, 1993, Phys. Rev. A **48**, R3433.
L'Huillier, A., K. J. Schafer, and K. C. Kulander, 1991, Phys. Rev. Lett. **66**, 2200.
Li, X. F., A. L'Huillier, M. Ferray, L. A. Lompré, and G. Mainfray, 1989, Phys. Rev. A **39**, 5751.
Liang, Y., A. Talebpuor, C. Y. Chien, S. Augst, and S. L. Chin, 1997, J. Phys. B **30**, 1369.
Lompré, L. A., A. L'Huillier, M. Ferray, P. Monot, G. Mainfray, and C. Manus, 1990, J. Opt. Soc. Am. B **7**, 754.
López-Martens, R., J. Mauritsson, P. Johnsson, K. Varjú, A. L'Huillier, W. Kornelis, J. Biegert, U. Keller, M. Gaarde, and K. Schafer, 2004, Appl. Phys. B: Lasers Opt. **78**, 835.
López-Martens, R., K. Varjú, P. Johnsson, J. Mauritsson, Y. Mairesse, P. Salières, M. B. Gaarde, K. J. Schafer, A. Persson, S. Svanberg, C.-G. Wahlström, and A. L'Huillier, 2005, Phys. Rev. Lett. **94**, 033001.
Lyngå, C., M. B. Gaarde, C. Delfin, M. Bellini, T. W. Hänsch, A. L'Huillier, and C.-G. Wahlström, 1999, Phys. Rev. A **60**, 4823.
Macklin, J. J., J. D. Kmetec, and C. L. Gordon III, 1993, Phys. Rev. Lett. **70**, 766.
Maiman, T. H., 1960, Nature (London) **187**, 493.
Mairesse, Y., *et al.*, 2003, Science **302**, 1540.
Mairesse, Y., *et al.*, 2004, Phys. Rev. Lett. **93**, 163901.
Maker, P. D., R. W. Terhune, M. Nisehoff, and C. M. Savage, 1962, Phys. Rev. Lett. **8**, 21.
Marcatili, E. A. J., and R. A. Schmeltzer, 1964, Bell Syst. Tech. J. **43**, 1783.
Mauritsson, J., P. Johnsson, E. Gustafsson, A. L'Huillier, K. J. Schafer, and M. B. Gaarde, 2006, Phys. Rev. Lett. **97**, 013001.
Mauritsson, J., P. Johnsson, R. López-Martens, K. Varjú, W. Kornelis, J. Biegert, U. Keller, M. B. Gaarde, K. J. Schafer, and A. L'Huillier, 2004, Phys. Rev. A **70**, 021801(R).
McPherson, A., R. Gibson, H. Jara, U. Johann, T. S. Luk, I. A. McInyre, K. Boyer, and C. K. Rhodes, 1987, J. Opt. Soc. Am. B **4**, 595.
Meshulach, D., and Y. Silberberg, 1998, Nature (London) **396**, 239.
Milošević, D., G. Paulus, D. Bauer, and W. Becker, 2006, J. Phys. B **39**, R203.
Miyamoto, N., M. Kamei, D. Yoshitomi, T. Kanai, T. Sekikawa, T. Nakajima, and S. Watanabe, 2004, Phys. Rev. Lett. **93**, 083903.
Moreno, P., L. Plaja, and L. Roso, 1997, Phys. Rev. A **55**, R1593.
Morlens, A.-S., P. Balcou, P. Zeitoun, C. Valentin, V. Laude, and S. Kazamias, 2005, Opt. Lett. **30**, 1554.
Muller, H., 2002, Appl. Phys. B: Lasers Opt. **74**, S17.
Murakami, M., J. Mauritsson, A. L'Huillier, K. J. Schafer, and M. B. Gaarde, 2005, Phys. Rev. A **71**, 013410.
Nisoli, M., S. D. Silvestri, and O. Svelto, 1996, Appl. Phys. Lett. **68**, 2793.
Norreys, P. A., *et al.*, 1996, Phys. Rev. Lett. **76**, 1832.
Nugent-Glandorf, L., M. Scheer, D. A. Samuels, A. M. Mulhisen, E. R. Grant, X. Yang, V. M. Bierbaum, and S. R. Leone, 2001, Phys. Rev. Lett. **87**, 193002.
Oron, D., Y. Silberberg, N. Dudovich, and D. M. Villeneuve, 2005, Phys. Rev. A **72**, 063816.
Papadogiannis, N. A., L. A. A. Nikolopoulos, D. Charalambidis, G. D. Tsakiris, P. Tzallas, and K. Witte, 2003, Phys. Rev. Lett. **90**, 133902.
Paul, A., R. A. Bartels, R. Tobey, H. Green, S. Weiman, I. P. Christov, M. M. Murnane, H. C. Kapteyn, and S. Backus, 2003, Nature (London) **421**, 51.
Paul, P. M., E. S. Toma, P. Breger, G. Mullot, F. Augé, P. Balcou, H. G. Muller, and P. Agostini, 2001, Science **292**, 1689.
Paulus, G. G., W. Becker, W. Nicklich, and H. Walther, 1994, J. Phys. B **27**, L703.
Paulus, G. G., W. Nicklich, H. Xu, P. Lambropoulos, and H. Walther, 1994, Phys. Rev. Lett. **72**, 2851.
Pfeifer, T., L. Gallmann, M. J. Abel, D. M. Neumark, and S. R. Leone, 2006, Opt. Lett. **31**, 975.
Pfeifer, T., R. Kemmer, R. Spitzenpfeil, D. Walter, C. Winterfeldt, G. Gerber, and C. Spielmann, 2005, Opt. Lett. **30**, 1497.
Pfeifer, T., D. Walter, G. Gerber, M. Y. Emelin, M. Y. Ryabikin, M. D. Chernobrovtseva, and A. M. Sergeev, 2004, Phys. Rev. A **70**, 013805.
Pfeifer, T., D. Walter, C. Winterfeldt, C. Spielmann, and G. Gerber, 2005, Appl. Phys. B: Lasers Opt. **80**, 277.
Pfeifer, T., U. Weichmann, S. Zipfel, and G. Gerber, 2003, J. Mod. Opt. **50**, 705.
Reitze, D. H., S. Kazamias, F. Weihe, G. Mullot, D. Douillet, F. Augé, O. Albert, V. Ramanathan, J. P. Chambaret, D. Hulin,

and P. Balcou, 2004, Opt. Lett. **29**, 86.
Roos, L., M. B. Gaarde, and A. L'Huillier, 2001, J. Phys. B **34**, 5041.
Rose, T. S., M. J. Rosker, and A. H. Zewail, 1988, J. Chem. Phys. **88**, 6672.
Rundquist, A., C. G. Durfee III, Z. Chang, C. Herne, S. Backus, M. M. Murnane, and H. C. Kapteyn, 1998, Science **280**, 1412.
Salières, P., P. Antoine, A. de Bohan, and M. Lewenstein, 1998, Phys. Rev. Lett. **81**, 5544.
Salières, P., B. Carré, L. Le Déroff, F. Grasbon, G. G. Paulus, H. Walther, R. Kopold, W. Becker, D. B. Milošević, A. Sanpera, and M. Lewenstein, 2001, Science **292**, 902.
Salières, P., A. L'Huillier, and M. Lewenstein, 1995, Phys. Rev. Lett. **74**, 3776.
Sansone G., P. Benedetti, F. Calegari, C. Vozzi, L. Avaldi, R. Flammini, L. Poletto, P. Villoresi, C. Altucci, R. Velotta, S. Stagiara, S. DeSilvestri, and M. Nisoli, 2006, Science **314**, 443.
Schafer, K. J., M. B. Gaarde, A. Heinrich, J. Biegert, and U. Keller, 2004, Phys. Rev. Lett. **92**, 023003.
Schnürer, M., Z. Cheng, M. Hentschel, G. Tempea, P. Kálmán, T. Brabec, and F. Krausz, 1999, Phys. Rev. Lett. **83**, 722.
Schnürer, M., C. Spielmann, P. Wobrauschek, C. Streli, N. H. Burnett, C. Kan, K. Ferencz, R. Koppitsch, Z. Cheng, T. Brabec, and F. Krausz, 1998, Phys. Rev. Lett. **80**, 3236.
Schwoerer, H., 2004, in *Femtosecond Technology for Technical and Medical Application*, edited by F. Dausinger, F. Lichter, and H. Lubatschowski, Topics in Applied Physics Vol. 96 (Springer, New York), p. 235.
Scrinzi, A., M. Y. Ivanov, R. Kienberger, and D. M. Villeneuve, 2006, J. Phys. B **39**, R1.
Sekikawa, T., A. Kosuge, T. Kanai, and S. Watanabe, 2004, Nature (London) **432**, 605.
Seres, E., J. Seres, F. Krausz, and C. Spielmann, 2004, Phys. Rev. Lett. **92**, 163002.
Seres, E., and C. Spielmann, 2007, Appl. Phys. Lett. **91**, 2789732.
Seres, J., E. Seres, A. J. Verhoef, G. Tempea, C. Streli, P. Wobrauschek, V. Yakovlev, A. Scrinzi, C. Spielmann, and F. Krausz, 2005, Nature (London) **433**, 596.
Shan, B., and Z. Chang, 2001, Phys. Rev. A **65**, 011804(R).
Shkolnikov, P. L., A. E. Kaplan, and A. Lago, 1996, J. Opt. Soc. Am. B **13**, 412.
Siegman, A. E., 1986, *Lasers*, 1st ed. (University Science Books, Sausalito, CA).
Silberberg, Y., 2001, Nature (London) **414**, 494.
Sola, I. J., E. Mevel, L. Elouga, E. Constant, V. Strelkov, L. Poletto, P. Villoresi, P. Benedetti, J. P. Caumes, S. Stagiara, C. Vozzi, G. Sansone, and M. Nisoli, 2006, Nat. Phys. **2**, 319.
Spielmann, C., N. H. Burnett, S. Sartania, R. Koppitsch, M. Schnürer, C. Kan, M. Lenzner, P. Wobrauschek, and F. Krausz, 1997, Science **278**, 661.
Spielmann, C., C. Kan, N. H. Burnett, T. Brabec, M. Geissler, A. Scrinzi, M. Schnürer, and F. Krausz, 1998, IEEE J. Sel. Top. Quantum Electron. **4**, 249.
Stapelfeldt, H., and T. Seideman, 2003, Rev. Mod. Phys. **75**, 543.
Strelkov, V. V., V. T. Platonenko, and A. Becker, 2005, Phys. Rev. A **71**, 053808.
Strelkov, V., A. Zaïr, O. Tcherbakoff, R. López-Martens, E. Cormier, E. Mével, and E. Constant, 2004, Appl. Phys. B: Lasers Opt. **78**, 879.
Sutherland, J. R., E. L. Christensen, N. D. Powers, S. E. Rhynard, J. C. Painter, and J. Peatross, 2004, Opt. Express **12**, 4430.
Tallents, G. J., 2003, J. Phys. D **36**, R259.
Tamaki, Y., J. Itatani, M. Obara, and K. Midorikawa, 2000, Phys. Rev. A **62**, 063802.
Tamaki, Y., Y. Nagata, M. Obara, and K. Midorikawa, 1999, Phys. Rev. A **59**, 4041.
Tate, J., T. Auguste, H. G. Muller, P. Saliers, P. Agostini, and L. F. DiMauro, 2007, Phys. Rev. Lett. **98**, 013901.
Tempea, G., and T. Brabec, 1998, Opt. Lett. **23**, 762.
Tempea, G., and T. Brabec, 2000, Appl. Phys. B: Lasers Opt. **70**, S197.
Tzallas, P., D. Charalambidis, N. A. Papadogiannis, K. Witte, and G. D. Tsakiris, 2003, Nature (London) **426**, 267.
Varjú, K., Y. Mairesse, B. Carré, M. B. Gaarde, P. Johnsson, S. Kazamias, R. López-Martens, J. Mauritsson, K. J. Schafer, P. Balcou, A. L'Huillier, and P. Saliéres, 2005, J. Mod. Opt. **52**, 379.
Verluise, F., V. Laude, Z. Cheng, C. Spielmann, and P. Tournois, 2000, Opt. Lett. **25**, 575.
Villoresi, P., S. Bonora, M. Pascolini, L. Poletto, G. Tondello, C. Vozzi, M. Nisoli, G. Sansone, S. Stagira, and S. D. Silvestri, 2004, Opt. Lett. **29**, 207.
Wabnitz, H., *et al.*, 2002, Nature (London) **420**, 482.
Walker, B., B. Sheehy, L. F. DiMauro, P. Agostini, K. J. Schafer, and K. C. Kulander, 1994, Phys. Rev. Lett. **73**, 1227.
Walter, D., T. Pfeifer, C. Winterfeldt, R. Kemmer, R. Spitzenpfeil, G. Gerber, and C. Spielmann, 2006, Opt. Express **14**, 3433.
Weihe, F. A., and P. H. Bucksbaum, 1996, J. Opt. Soc. Am. B **13**, 157.
Weinacht, T. C., J. L. White, and P. H. Bucksbaum, 1999, J. Phys. Chem. A **103**, 10166.
Weiner, A. M., 2000, Rev. Sci. Instrum. **71**, 1929.
Weiner, A. M., D. E. Leaird, J. S. Patel, and J. R. Wullert, 1990, Opt. Lett. **15**, 326.
Xiao, J., Z. Sun, X. Zhang, Y. Wang, W. Zhang, Z. Wang, R. Li, and Z. Xu, 2006, J. Opt. Soc. Am. B **23**, 771.
Yamane, K., Z. Zhang, K. Oka, R. Morita, M. Yamashita, and A. Suguro, 2003, Opt. Lett. **28**, 2258.
Yedder, A. B. H., C. Le Bris, O. Atabek, S. Chelkowski, and A. D. Bandrauk, 2004, Phys. Rev. A **69**, 041802(R).
Yelin, D., D. Meshulach, and Y. Silberberg, 1997, Opt. Lett. **22**, 1793.
Yoshitomi, D., J. Nees, N. Miyamoto, T. Sekikawa, T. Kanai, G. Mourou, and S. Watanabe, 2003, Appl. Phys. B: Lasers Opt. **78**, 275.
Zair, A., O. Tcherbakoff, E. Mevel, E. Constant, R. Lopez-Martens, J. Mauritsson, P. Johnsson, and A. L'Huillier, 2004, Appl. Phys. B: Lasers Opt. **78**, 869.
Zeek, E., K. Maginnis, S. Backus, U. Russek, M. Murnane, G. Mourou, H. Kapteyn, and G. Vdovin, 1999, Opt. Lett. **24**, 493.
Zewail, A. H., 2000, J. Phys. Chem. A **104**, 5660.